A Wideband Fast Multipole Method for the Helmholtz kernel: Theoretical developments

Stéphanie Chaillat, Francis Collino

A Wideband Fast Multipole Method for the Helmholtz kernel: Theoretical developments

Stéphanie Chaillat, Francis Collino

RESEARCH REPORT
N° 8692
March 2015
Project-Teams POEMS

ISSN 0249-6399 ISRN INRIA/RR--8692--FR+ENG

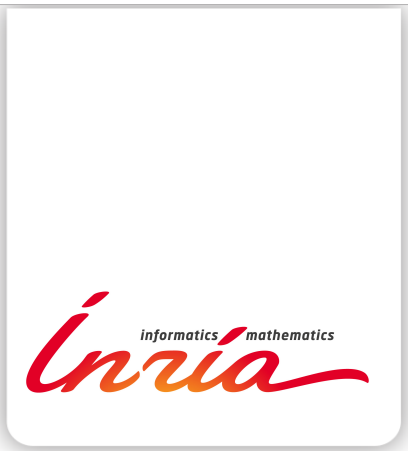

A Wideband Fast Multipole Method for the Helmholtz kernel: Theoretical developments

Stéphanie Chaillat*, Francis Collino†

Project-Teams POEMS

Research Report n° 8692 — March 2015 — 28 pages

Abstract: This work presents a new Fast Multipole Method (FMM) based on plane wave expansions, combining the advantages of the low and high frequency formulations. We revisit the method of Greengard et al. devoted to the low frequency regime and based on the splitting of the Green's function into a propagative and an evanescent part. More precisely, we give an explicit formula of the filtered translation function for the propagative part, we derive a new formula for the evanescent part and we provide a new interpolation algorithm. At all steps, we check the accuracy of the method by providing error estimates. These theoretical developments are used to propose a wideband FMM based entirely on plane wave expansions. The numerical efficiency and accuracy of this broadband are illustrated with a numerical example.

Key-words: Fast Multipole Method, Quadrature errors,Plane wave expansion, Helmholtz equation, Broadband

* POEMS (UMR 7231 CNRS-ENSTA-INRIA), ENSTA Paristech, France (stephanie.chaillat@ensta.fr)
† CERFACS, 42 avenue G. Coriolis, 31057 Toulouse, France (francis.collino@orange.fr)

RESEARCH CENTRE
SACLAY – ÎLE-DE-FRANCE

1 rue Honoré d'Estienne d'Orves
Bâtiment Alan Turing
Campus de l'École Polytechnique
91120 Palaiseau

Une méthode multipôle rapide pour le noyau d'Helmholtz stable et efficace pour toutes fréquences : Développements théoriques

Résumé : Ce travail présente une nouvelle méthode multipôle rapide basée sur un développement en ondes planes qui combine les avantages des formulations hautes et basses fréquences. Nous améliorons la méthode basse fréquence de Greengard et al. basée sur une décomposition de la fonction de Green en une partie propagative et une partie évanescente. Plus précisément, nous donnons une formule explicite de la fonction de transfert filtrée pour la partie de propagative, nous dérivons une nouvelle expression de la partie évanescente et nous fournissons un nouvel algorithme d'interpolation. A chaque étape, nous vérifions la précision de la méthode en fournissant des estimations d'erreur. Ces développements théoriques sont utilisés pour proposer une FMM toutes fréquences entièrement basée sur un développement en ondes planes. L'efficacité numérique et la précision de cette méthode toutes fréquences sont illustrées sur un exemple numérique.

Mots-clés : Méthode multipôle rapide, erreurs de quadrature, développement en ondes planes, équation d'Helmholtz, méthode toute fréquence

Contents

1 Introduction

Let X be a cloud of points in $\mathbb{R}^3$ and k a real wavenumber; we consider the Helmholtz potential induced by the charges ρ_i located at the points $x_i \in X$,

$$V_i = \sum_{j \neq i} \frac{e^{ik|x_i - x_j|}}{|x_i - x_j|} \rho_j = \sum_{j \neq i} \mathbb{G}_{ij} \rho_j, \quad x_i \in X. \tag{1}$$

When the number N of points in X is large, computing this matrix-vector product is prohibitive due to the CPU and storage costs. The Fast Multipole Method (`FMM`) was developed in the 1980s to speed up this computation and reduce the memory requirements. The idea is to compute this matrix-vector product in a fast and approximate way while keeping the error below a prescribed level. The original FMM proposed by Rokhlin in [25] relies on a truncated multipole expansion for the approximation of the Green's function. In [26], Rokhlin proposed the diagonal forms of the translation operators for the 3D Helmholtz equation. The complete mathematical justification can be found in [14]. Competitive methods to the FMM have been proposed in the recent years. Their main advantage is the straightforward extension to any kernel since they do not require an analytical expansion. For example, Fong and Darve proposed in [15] a "black box FMM" for non-oscillatory kernels based on a Chebyshev interpolation scheme. The method is extended to oscillatory kernels in [22]. Another kernel-independent FMM was proposed by Engquist and Ying [13]. All these techniques take advantage of low-rank properties of some blocks in the matrix. Recently, methods based on hierarchical matrices [18] to derive the low rank approximations have emerged. For oscillatory kernels, it has been shown empirically that it is a useful tool for moderate frequencies [21]. However, the FMM is still a viable and interesting procedure due to its sound mathematical background for oscillatory kernels. In this paper, we show (by providing error estimates) how to tune carefully the various parameters of the method.

The diagonalization of the original FMM introduced in [26] paved the way for an approach based on an expansion using propagative plane waves (`PWFMM`) [7, 9]. We call this approach the high frequency `PWFMM` (`HF-PWFMM`) because the translation operators become unstable when the characteristic spatial lengths are smaller than the wavelength [24, 19, 6]. To overcome this drawback and handle lower frequencies, Bogaert and Olyslager [2] constructed an *ad hoc* procedure well adapted to low frequencies. A different approach is proposed by Greengard et al. [16]. The idea is to add evanescent waves to the plane wave expansion, leading to the low frequency `PWFMM` (`LF-PWFMM`). The `LF-PWFMM` was then studied and improved on, in several directions, for example by Darve and Havé [11], Wallen et *al.* [28]. Although more computationally expensive than the `HF-PWFMM`, the `LF-PWFMM` produces stable computations for low frequency problems.

Since the `HF-PWFMM` is not accurate for the lower frequencies and the `LF-PWFMM` is more expensive for the higher frequencies, it is ineffective to use the same formulation for all the frequencies. The idea is to couple the `HF` and `LF` formulations and to use the `HF` method whenever possible. Such formulations are called wideband or broadband FMMs. In [5], a wideband FMM was proposed by Cheng et al. It uses the original FMM proposed by Rokhlin. To take advantage of the diagonal *far field to local* translation operators for the lower frequencies, a conversion between the traditional FMM and the `LF-PWFMM` is performed. A variant of this approach, avoiding the conversion to the `LF-PWFMM` was proposed by Gumerov and Duraiswami in [17].

The present works focus on the `PWFMM`. In a first part, we perform an extensive theoretical study of the `LF-PWFMM` and propose some improvements. Using this new formulation, we derive a wideband `PWFMM`. An outstanding feature of this wideband `PWFMM` is that *the far field to local* translations are intrinsically performed at all levels by means of diagonal operators. As a result, the implementation is simple.

Principle of the `PWFMM` The `PWFMM` is presented in several monographs [6] and papers (see for example [7, 9]). In [12], a detailed connection between the `PWFMM` and the *FMM* based on a multipole expansion is proposed. Basically in the `PWFMM` (see for example in [9]), the translations refer exclusively to the diagonal form of the *far field to local translations* of Rokhlin's FMM (the translations between cells at the same level); and the interpolation step (together with a phase shift) corresponds to the *far field to far field* and *local to local* translations.

We now recall the basic ideas of the `PWFMM`; for more details, the interested reader is referred to [10]. In a first step, a 3D cubic grid of linear spacing D, embedding the cloud of points X, is created; the cubic cells are then recursively subdivided into eight smaller cubic cells; the cell-subdivision approach is systematized by means of an octree. At each level ℓ, the linear cell size is $d = \frac{D}{2^\ell}$, $\ell = 1, ..., \pounds$. The octree is used to derive a block decomposition of the matrix $\mathbb{G}$. Generally speaking, the definition of an efficient `PWFMM` is based on the following three ingredients:

1. An approximation formula for the evaluation of the Green's function in terms of plane waves. If $x \in B_t$ and $y \in B_s$, the Green's function is sought under the form

$$\frac{e^{ik|x_t - y_s|}}{|x_t - y_s|} \simeq \int_{\hat{\Lambda}} T(\vec{k}; \vec{t})\, e^{i\vec{k}\cdot((x_t - c_t)-(y_s - c_s))}\, d\hat{\Lambda}(\vec{k}),\ x_t \in B_t,\ y_s \in B_s$$
$$\text{with } \hat{\Lambda} \subset \left\{ \vec{k} = (k_x, k_y, k_z) \in \mathbb{C}^3,\ k_x^2 + k_y^2 + k_z^2 = k^2 \right\} \tag{2}$$

   where $\vec{k}$ is a wave vector, $\vec{t} = c_t - c_s$ is the translation vector linking the centers of two interacting cells (B_s, B_t) and T is the translation function. Due to the octree structure, the translation vectors are defined by $\vec{t} = (id, jd, md)$ with $|i|, |j|, |m| \leq 3$ and $|i|+|j|+|m| > 3$. As a result, the number of possible translation vectors at a given level is finite and bounded by $7^3 - 3^3 = 316$ (see [10] for more details).

2. Accurate quadrature rules for the evaluation of the integrals over $\hat{\Lambda}$. These quadrature rules will depend only on the size of the cells at a given level. Consequently there are as many quadrature rules as there are levels in the octree.

3. An interpolation formula allowing the evaluation of the plane waves at the level-ℓ quadrature points from their values at the level-$(\ell - 1)$ quadrature points. This last ingredient yields some additional factorizations of the computations, as the contributions at level-ℓ are reused to evaluate the contributions at level-$(\ell - 1)$ [9].

In the `HF-PWFMM`, the plane wave expansion is defined only in terms of propagative waves, reducing $\hat{\Lambda}$ in (2) to the unit sphere in $\mathbb{R}^3$ (i.e. $\hat{\Lambda} = kS^2$). In this case, the translation function is a series involving spherical Hankel functions which are known to increase exponentially for small arguments. As a result, the `HF-PWFMM` suffers from numerical breakdowns in the low frequency regime. In the `LF-PWFMM`, the evanescent plane waves are added to the expansion leading to a more expensive but also more stable method [10]. This extra cost is due to the introduction of six distinct factorizations in the `LF-PWFMM` instead of one in the `HF-PWFMM` [16]. Accordingly, the 316 translation vectors are dispatched into these six directions (with at most 74 translation vectors within a group).

Proposed improvements. The main contributions presented are the following:

1. Error estimates of the main steps of the algorithm.

2. An explicit formula to evaluate the translation function for the propagative part.

3. A new formula for the evanescent part, allowing to simplify the `LF-PWFMM` previously proposed [16, 11] by amounting the evanescent part to the static case.
4. A new interpolation algorithm for the evanescent plane waves.
5. A new `PWFMM` combining the advantages of the low and high frequency formulations.

Outline. In Section 2, we introduce the new stable plane wave expansion. Then in Sections 3 and 4, we study the propagative and the evanescent parts respectively. Namely, the plane wave expansions are given in (19) and (38), the translation functions in (25) and (37). In Section 5, we present a `PWFMM`, which is stable at all frequencies and efficient from the low to the high frequencies. Finally, in Section 6, a numerical example is given to illustrate the capabilities of the method.

2 New stable plane wave expansions

The first ingredient to define an efficient `PWFMM` is the derivation of an approximation formula for the Green's function, in terms of plane waves. The common tool to all the `LF-PWFMM`s [16, 11, 5] is the Sommerfeld formula. Let $\vec{w}$ be a vector with $z_w > 0$. In the following, $\vec{w}$ denotes a vector, (x_w, y_w, z_w) its Cartesian coordinates in $(0, \hat{x}, \hat{y}, \hat{z})$, $(R_w = |\vec{w}|, \theta_w, \varphi_w)$ its spherical coordinates, and $(r_w = R_w \sin\theta_w, \varphi_w, z_w)$ its cylindrical coordinates; In [5], the Green's function is written as

$$\frac{e^{ik|\vec{w}|}}{|\vec{w}|} = \frac{1}{2\pi}\int_0^\infty e^{-\sqrt{\lambda^2-k^2}z_w} J_0(\lambda r_w)\frac{\lambda}{\sqrt{\lambda^2-k^2}}\,d\lambda. \tag{3}$$

In this work, we choose to split the Green's function into the following two parts ([27], [29, p. 416])

$$\frac{e^{ik|\vec{w}|}}{|\vec{w}|} = G_p(\vec{w}) + G_e(\vec{w}),$$

with the propagative part G_p, respectively the evanescent part G_e, given by

$$G_p(\vec{w}) = ik\int_0^{\frac{\pi}{2}} J_0(kr_w\sin\theta)e^{ikz_w\cos\theta}\sin\theta d\theta, \tag{4}$$

$$G_e(\vec{w}) = \int_0^\infty J_0(\sqrt{\lambda^2+k^2}r_w)e^{-\lambda z_w}\,d\lambda, \tag{5}$$

where $J_0(t)$ is the Bessel function of order 0. It is possible to evaluate these two functions in a simple and accurate way since both the propagative (4) and the evanescent (5) parts can be written as fast convergent series. The propagative part is given by [20]

$$G_p(\vec{w}) = -k\sum_{q=0}^{\infty}\tilde{\beta}_{2q+1}j_{2q+1}(kR_w)P_{2q+1}(\frac{z_w}{R_w}) + i\frac{\sin kR_w}{R_w} \tag{6}$$

where $P_n(t)$ is the *Legendre polynomial* of degree n, $j_n(u)$ is the spherical Bessel function [8] while the coefficients $\tilde{\beta}_{2q+1}$ are

$$\tilde{\beta}_{2q+1} = (-1)^q\frac{P_{2q}(0)}{2q+2}\left(2(2q+1)+1\right) = \frac{2(2q+1)+1}{2q+2}\,\frac{1.3...(2q-1)}{2.4....2q}.$$

Similarly, the evanescent part is [29, p.358 & 386]

$$G_e(\vec{w}) = \frac{1}{R_w}\sum_{p=0}^{\infty}(-1)^p \varepsilon_p J_{2p}(kr_w)\Big[\cot\left(\frac{\Psi_w}{2}\right)\Big]^{2p}, \quad \cot\left(\frac{\Psi_w}{2}\right) = \frac{R_w - z_w}{r_w} \tag{7}$$

where ε_p is *the Neumann factor* defined by $\varepsilon_p = 2$ when $p \neq 0$ and $\varepsilon_0 = 1$. These formulas are given here mainly to check the accuracy of the approximations of either G_p or G_e.

The approach proposed by Greengard et al. in [16] to accelerate (and approximate) the evaluation of the Green's function in (1) is based on the representation of the Bessel functions [29, p. 19]

$$J_0(t) = \frac{1}{2\pi}\int_0^{2\pi} e^{it\cos(\varphi-\psi)}\, d\varphi, \qquad \text{for any angle } \psi. \tag{8}$$

Taking $\psi = \varphi_w$ and plugging (8) into (4), the propagative part is found in terms of plane waves

$$G_p(\vec{w}) = \frac{ik}{2\pi}\int_0^{\frac{\pi}{2}}\int_0^{2\pi} e^{ikR_w(\cos\theta\cos\theta_w + \sin\theta_w\sin\theta\cos(\varphi-\varphi_w))}\sin\theta d\theta d\varphi = \frac{ik}{2\pi}\int_{S^2}\pi(\hat{s})e^{ik\hat{s}\cdot\vec{w}}\, d\sigma(\hat{s}) \tag{9}$$

where S^2 is the unit sphere, and $\pi(\hat{s})$ is the characteristic function of the upper hemisphere, i.e. of the directions oriented toward $0z$

$$\pi(\hat{s}) = 1 \;\text{ if }\; \hat{s}\cdot\hat{z} \geq 0 \quad \text{ and } \quad = 0 \;\text{ if }\; \hat{s}\cdot\hat{z} < 0. \tag{10}$$

Similarly, the evanescent part may be recast as

$$G_e(\vec{w}) = \frac{1}{2\pi}\int_0^{\infty}\int_0^{2\pi} e^{i\vec{k}(\lambda,\varphi)\cdot\vec{w}}\, d\varphi d\lambda \quad \text{ with } \quad \vec{k} = \begin{bmatrix} \sqrt{k^2+\lambda^2}\cos\varphi \\ \sqrt{k^2+\lambda^2}\sin\varphi \\ i\lambda \end{bmatrix}. \tag{11}$$

Definition of appropriate and accurate quadrature rules. In the context of the `PWFMM`, the plane wave expansions are used to evaluate the contributions coming from interacting pairs of cells (B_s, B_t). The formulas (9) and (11) are applied in the special case where $\vec{w} = \vec{t} + \vec{v}$, $\vec{t} = c_t - c_s$ and $\vec{v} = x - c_t - y + c_s$. This implies for the group associated to the evanescence axis Oz that the 74 translation vectors are defined by $\vec{t} = (id, jd, md)$ with $|i|, |j| \leq m$ and $m = 2$ or 3 (where d is the length of the edges of the cells). Since the three coordinates of the vector $\vec{v}$ lie between $-d$ and d, we have in addition $\vec{w} \in \Omega_d = d\hat{\Omega}$, and $\hat{\Omega}$ is the set given by (Fig. 1)

$$\hat{\Omega} = \Big\{(\hat{r}_w, \hat{z}_w) \in [0, 3\sqrt{2}] \times [1,3] \cup [0, 4\sqrt{2}] \times [2,4]\Big\}. \tag{12}$$

Having reduced the size of the domain of definition of the vector $\vec{w}$, the key point in the `LF-PWFMM` is the definition of accurate quadrature rules for (11) for all $\vec{w} \in \Omega_d$, with a small number of quadrature points (to optimize the computational costs). Since the phase of the integrand in (11) is nonlinear with respect to λ, deriving an optimal quadrature rule (in the sense of accuracy and number of points) is a difficult problem. There are various approaches in the literature. For example in [5], an optimal Generalized Gaussian quadrature is obtained to integrate (3) by using the methodology proposed by Yarvin and Rokhlin in [30]. A similar approach is used in [11] for the integration of the evanescent part (11). The minor drawback of these approaches is the need for each problem to pre-compute the appropriate quadrature rules. In [28], Wallén et al. provided quadrature points and weights for several values of d ($kd = \frac{2\pi}{2^\ell}$, $\ell = 0, ..., 8$) and different levels of accuracy. The drawback of this last approach is the constraint on the length

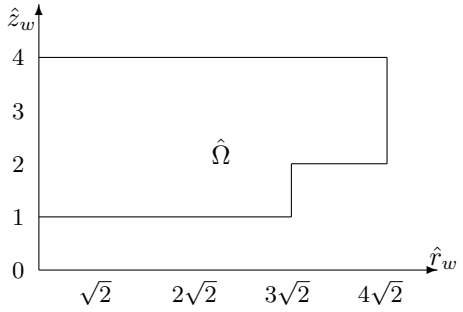

Figure 1: Definition of the normalized domain $\hat{\Omega}$ in which the vectors $\vec{w}/d$ lie, i.e. $\vec{w} \in \Omega_d$.

of the largest cell. The main issue to define an efficient `LF-PWFMM` is then the construction of an efficient interpolation algorithm.

In this work, we propose a method to avoid these drawbacks by simplifying the derivation of the quadrature rule and interpolation algorithm for the evanescent part. The idea is to reformulate (11) by using a clever change of variables. The starting point is to note that the integral representation of the Bessel functions (8) is valid for any angle ψ. Instead of $\psi = \varphi_w$, we use the angle $\psi = \varphi_w + \psi_{\lambda,k}$ with

$$\cos\psi_{\lambda,k} = \frac{k}{\sqrt{\lambda^2+k^2}} \quad \text{and} \quad \sin\psi_{\lambda,k} = \frac{\lambda}{\sqrt{\lambda^2+k^2}}. \tag{13}$$

Inserting the formula (8) in (5), with ψ given as above, and using simple trigonometric formulas; the evanescent part now reads

$$G_e(\vec{w}) = \frac{1}{2\pi}\int_0^\infty \int_0^{2\pi} e^{i\vec{k}(\lambda,\varphi)\cdot\vec{w}}\, d\varphi d\lambda \quad \text{with} \quad \vec{k} = \begin{bmatrix} k\cos\varphi + \lambda\sin\varphi \\ k\sin\varphi - \lambda\cos\varphi \\ i\lambda \end{bmatrix}. \tag{14}$$

This rotation by an angle $\psi_{\lambda,k}$ (which depends on λ) leads to a phase which is linear with respect to λ. We will prove in Section 4 that some important simplifications follow from this new expression:

1. It is possible to use the optimal quadrature rules designed for the static case (for $k = 0$).
2. A fast interpolation algorithm similar to the one proposed on the unit sphere for the `HF-PWFMM` is easily derived.
3. Error estimates on the main steps of the `PWFMM` are obtained.

Before presenting the improvements on the evanescent part, we discuss the propagative part in the next section.

3 Numerical evaluation of the propagative part of the Green's function

We follow the same strategy as in Darve and Havé [11]. The difficulty to integrate numerically (9) is due to the discontinuity at $z = 0$. The main idea is to replace the upper hemisphere (10) with the complete sphere and to filter out the higher harmonic modes of the translation function. With this strategy, we reduce the number of plane wave expansions from six (for the six axes

of evanescence) to one; as a consequence, the CPU time is also reduced. The second advantage is the possibility to use both the quadrature rules and the interpolation step designed for the `HF-PWFMM` [10]. In the following, we propose (i) estimates on the error introduced by the quadrature rule to perform the integration on the unit sphere and (ii) a new expression of the translation function.

3.1 Estimations of the errors introduced by the quadrature rules

Mathematical preliminaries. $P_n^\mu(x)$ denotes the *associated Legendre functions* of argument x, order n and momentum μ, i.e. $P_n^\mu(x) = (1-x^2)^{\frac{\mu}{2}} \frac{d^\mu P_n(t)}{dx^\mu}$. It is known [8, Theorem 2.7], that *the spherical harmonics*

$$Y_n^m(\theta,\varphi) = \sqrt{\frac{2n+1}{4\pi}} \sqrt{\frac{(n-|m|)!}{(n+|m|)!}} P_n^{|m|}(\cos\theta) e^{im\varphi} \text{ for } m=-n,\dots,n,\ n\geq 0 \tag{15}$$

form a complete orthonormal system in $L^2(S^2)$. In (15), we choose the spherical coordinate system defined by

$$x = \sin\theta\cos\varphi,\ y = \sin\theta\sin\varphi,\ z = \cos\theta. \tag{16}$$

Let L be a non negative integer, the mapping $\Pi^L : L^2(S^2) \to L^2(S^2)$

$$\Pi^L f(\hat{s}) = f^L(\hat{s}) = \sum_{\ell=0}^{L} \sum_{m=-\ell}^{\ell} \left(\int_{S^2} f(\hat{d}) \overline{Y_l^m(\hat{d})}\, d\sigma(\hat{d}) \right) Y_l^m(\hat{s}) \tag{17}$$

defines an orthogonal projector in $L^2(S^2)$ onto the spherical harmonics of degree less than or equal to L. The following lemma will be useful to derive the quadrature rules.

Lemma 3.1 *Let $E(\hat{s})$ be a continuous function defined on the unit sphere S^2. Define the errors*

$$\varepsilon_\infty^L = \sup_{\hat{s}\in S^2} \left| E(\hat{s}) - \Pi^L E(\hat{s}) \right| \quad \text{and} \quad \varepsilon_2^L = \left(\frac{1}{4\pi} \int_{S^2} \left| E(\hat{s}) - \Pi^L E(\hat{s}) \right|^2 \right)^{\frac{1}{2}}. \tag{18}$$

Let $\oint_{S^2}$ be a quadrature rule over the unit sphere, exact for the spherical harmonics of degree less than or equal to $2L+1$, then for all square integrable functions $T(\hat{s})$, the quadrature error

$$\varepsilon^L = \frac{1}{4\pi} \int_{S^2} T(\hat{s}) E(\hat{s}) - \frac{1}{4\pi} \oint_{S^2} \Pi^L T(\hat{s}) E(\hat{s})$$

satisfies the bound $|\varepsilon^L| \leq \|T\|_2 \left(\varepsilon_\infty^{L+1} + \varepsilon_2^L \right)$ *with* $\|T\|_2 = \left(\frac{1}{4\pi} \int_{S^2} |T(\hat{s})|^2 \right)^{\frac{1}{2}}$.

Proof: Let $\Pi_\perp^L$ be the orthogonal projector $I - \Pi^L$. It is straightforward that

$$\frac{1}{4\pi} \int_{S^2} T(\hat{s}) E(\hat{s}) = \frac{1}{4\pi} \int_{S^2} \Pi^L T(\hat{s}) \Pi^L E(\hat{s}) + \frac{1}{4\pi} \int_{S^2} \Pi_\perp^L T(\hat{s}) \Pi_\perp^L E(\hat{s}).$$

Due to the orthogonality of the spherical harmonics, we also have

$$\frac{1}{4\pi} \int_{S^2} T(\hat{s}) E(\hat{s}) = \frac{1}{4\pi} \int_{S^2} \Pi^L T(\hat{s}) \Pi^{L+1} E(\hat{s}) + \frac{1}{4\pi} \int_{S^2} \Pi_\perp^L T(\hat{s}) \Pi_\perp^L E(\hat{s}).$$

Then, $\Pi^L T(\hat{s})\Pi^{L+1}E(\hat{s})$ is the product of a spherical harmonic function of degree less than or equal to L and a spherical harmonic function of degree less than or equal to $L+1$. This product is a sum of spherical harmonics of degree less than or equal to $2L+1$. Since we have made the assumption that the quadrature rule integrates exactly the harmonic functions of degree less than or equal to $2L+1$, we get

$$\frac{1}{4\pi}\int_{S^2} T(\hat{s})E(\hat{s}) = \frac{1}{4\pi}\fint_{S^2}\Pi^L T(\hat{s})\Pi^{L+1}E(\hat{s}) + \frac{1}{4\pi}\int_{S^2}\Pi^L_\perp T(\hat{s})\Pi^L_\perp E(\hat{s}).$$

Then, using the decomposition $\Pi^{L+1}E = E - \Pi^{L+1}_\perp E$, we obtain

$$\varepsilon^L = -\frac{1}{4\pi}\fint_{S^2}\Pi^L T(\hat{s})\Pi^{L+1}_\perp E(\hat{s}) + \frac{1}{4\pi}\int_{S^2}\Pi^L_\perp T(\hat{s})\Pi^L_\perp E(\hat{s}).$$

Using the Cauchy-Schwartz inequality, it follows

$$|\frac{1}{4\pi}\fint_{S^2}\Pi^L T(\hat{s})\Pi^{L+1}_\perp E(\hat{s})| \leq \left(\frac{1}{4\pi}\fint_{S^2}\left|\Pi^L T(\hat{s})\right|^2\right)^{\frac{1}{2}} \left(\frac{1}{4\pi}\fint_{S^2}\left|\Pi^{L+1}_\perp E(\hat{s})\right|^2\right)^{\frac{1}{2}}$$

$$\text{and} \quad |\frac{1}{4\pi}\int_{S^2}\Pi^L_\perp T(\hat{s})\Pi^L_\perp E(\hat{s})| \leq \varepsilon_2^L \left\|\Pi^L_\perp T\right\|_2 .$$

Furthermore, due to the assumption on the quadrature rule, we have

$$\left(\frac{1}{4\pi}\fint_{S^2}\left|\Pi^L T(\hat{s})\right|^2\right)^{\frac{1}{2}} = \left(\frac{1}{4\pi}\int_{S^2}\left|\Pi^L T(\hat{s})\right|^2\right)^{\frac{1}{2}}.$$

Finally, we obtain the bound $|\frac{1}{4\pi}\fint_{S^2}\Pi^L T(\hat{s})\Pi^{L+1}_\perp E(\hat{s})| \leq \|\Pi^L T\|_2\, \varepsilon_\infty^{L+1}$.

It follows that $|\varepsilon^L| \leq \|\Pi^L_\perp T\|_2\, \varepsilon_2^L + \|\Pi^L T\|_2\, \varepsilon_\infty^{L+1}$ and the result follows since both $\|\Pi^L_\perp T\|_2$ and $\|\Pi^L T\|_2$ are bounded by $\|T\|_2$. ■

Error introduced by the quadrature rule in the propagative part. It is now possible to establish an estimate of the error introduced by the quadrature rule to evaluate the propagative part (9) and to determine the appropriate quadrature rule to minimize this error.

Proposition 3.1 *Let* $\fint_{S^2}$ *be a quadrature rule over the unit sphere, exact for the spherical harmonics of degree less than or equal to* $2L+1$. *Let* G_p^L *be defined by*

$$G_p^L(\vec{t},\vec{v}) = \fint_{S^2}\Pi^L\Big(\frac{ik}{2\pi}\pi(\hat{s})e^{ik\hat{s}\cdot\vec{t}}\Big)\, e^{ik\hat{s}\cdot\vec{v}}\, d\sigma(\hat{s}) = \frac{1}{4\pi}\fint_{S^2}\Pi^L\Big(T(\hat{s})\Big)E(\hat{s}). \tag{19}$$

Similarly to Lemma 3.1, we introduce the errors (18). With $E(\hat{s}) = e^{ik\hat{s}\cdot\vec{v}}$ *they are given by*

$$\varepsilon_\infty^L(kv) = kv\left(j_L^2(kv) + j_{L+1}^2(kv)\right)^{\frac{1}{2}} \quad \textit{and} \tag{20a}$$

$$\varepsilon_2^L(kv) = \frac{kv}{\sqrt{2}}\left(j_L^2(kv) - j_{L+1}(kv)j_{L-1}(kv) + j_{L+1}^2(kv) - j_{L+2}(kv)j_L(kv)\right)^{\frac{1}{2}}. \tag{20b}$$

Assuming that $|kv| \leq \sqrt{3}kd < L$ *and that*

$$4\sqrt{6}kd\left(\varepsilon_2^L(\sqrt{3}kd) + \varepsilon_\infty^{L+1}(\sqrt{3}kd)\right) < \varepsilon \tag{21}$$

then the approximation of $G_p(\vec{v}+\vec{t})$ satisfies the bound

$$\max_{\vec{t}+\vec{v}\in\Omega_d} |\vec{v}+\vec{t}||G_p^L(\vec{t},\vec{v}) - G_p(\vec{v}+\vec{t})| \leq \varepsilon. \tag{22}$$

Proof: In the context of the PWFMM, the propagative part is given by

$$G_p(\vec{t},\vec{v}) = \frac{ik}{2\pi}\int_{S^2} \pi(\hat{s}) e^{ik\hat{s}\cdot\vec{t}}\, e^{ik\hat{s}\cdot\vec{v}}\, d\sigma(\hat{s}) = \frac{1}{4\pi}\int_{S^2} T(\hat{s})E(\hat{s})$$

where $\vec{t}$ is the translation vector, $T(\hat{s}) = 2ik\pi(\hat{s})\, e^{ik\vec{t}\cdot\hat{s}}$ ($||T||_2 = \sqrt{2}k$) and $E(\hat{s}) = e^{ik\vec{v}\cdot\hat{s}}$. Using the Jacobi-Anger Formula, we have

$$E(\hat{s}) - \Pi^L E(\hat{s}) = \sum_{n=L+1}^{\infty} i^n(2n+1)j_n(kv)P_n(\hat{s}\cdot\hat{v}), \quad \vec{v} = v\hat{v}.$$

Assuming $L > kv$, the maximum error in the expansion is reached when $\hat{s} = \hat{v}$ [3]. Indeed,

$$\sum_{n=L+1}^{\infty} i^n(2n+1)j_n(kv) = i^{L+1}kv\left(j_L(kv) + ij_{L+1}(kv)\right)$$

and error estimate (20a) follows when $L > kv$. Similarly, the L^2 error is given by (20b) [3]. Assuming that the quadrature rule is exact for all the harmonic functions of degree less than or equal to $2L+1$, we apply Lemma 3.1 and obtain the estimate

$$|G_p^L(\vec{t},\vec{v}) - G_p(\vec{v}+\vec{t})| \leq \sqrt{2}k\left(\varepsilon_2^L(kv) + \varepsilon_\infty^{L+1}(kv)\right) \quad \text{with } \varepsilon_\infty^L,\ \varepsilon_2^L \text{ given in (20a), (20b).} \tag{23}$$

Through estimate (23), it is clear that the error increases when the modulus of $\vec{v}$ increases. Reminding that in the PWFMM, the vector $\vec{v}$ lies in a cell of center 0 and of size $2d$, then $kv \leq \sqrt{3}kd$ and the error estimate becomes

$$|G_p^L(\vec{t},\vec{v}) - G_p(\vec{v}+\vec{t})| \leq \sqrt{2}k\left(\varepsilon_2^L(\sqrt{3}kd) + \varepsilon_\infty^{L+1}(\sqrt{3}kd)\right). \tag{24}$$

Finally since $|\vec{t}+\vec{v}|$ is bounded by $4\sqrt{3}d$ the estimate follows. ■

An asymptotic analysis for small values of kd shows that error estimate (21) is in the order of $\varepsilon^{2L+1} = O\left((kd)^{2L+1}\right)$. As a result, the error decreases rapidly when L increases. In practice, the choice of the quadrature rule is dictated by the choice of L, the order of truncation in the translation function. Finally, the design of an accurate quadrature rule for the propagative part reduces to the choice of a quadrature rule exact for the spherical harmonics of degree less than or equal to $2L+1$. We choose the usual quadrature rule [9] with $N_\theta = L+1$ Gauss Legendre points in θ and $N_\varphi > 2L$ equidistributed points in φ. Other choices are possible (see [4]). In practice, estimate (21) provides an upper bound of the error associated to a given L. We report in Table 1 the minimum number of modes $L_{\text{theo.}}$ given by (21) to achieve an accuracy of 10^{-3}, 10^{-6}, 10^{-9} or 10^{-12} for five possible cell sizes. In addition, we report the number of modes $L_{\text{num.}}$ obtained numerically: we sample the faces of a cell with 600 vectors $\vec{v}$ and compute the error (22) for all the possible vectors $\vec{t}$; as long as the error remains below the prescribed level, $L_{\text{num.}}$ is decreased. The parameter $L_{\text{num.}}$ obtained during these numerical experiments is always slightly overestimated by $L_{\text{theo.}}$. Even though error estimate (21) does not give directly the minimum number of points, it is a good starting point to determine numerically the smallest value of $L_{\text{num.}}$ to achieve a prescribed accuracy. This method is reliable and fast. This estimate is an important feature to establish the method theoretically and to determine in practice an appropriate quadrature.

		$d=0$	$d=\lambda/8$	$d=\lambda/4$	$d=\lambda/2$	$d=\lambda$
$\varepsilon=10^{-3}$	$L_{\text{theo.}}$	0 (0)	6 (91)	8 (153)	13 (378)	21 (946)
	$L_{\text{num.}}$	0 (0)	5 (66)	7 (120)	11 (276)	19 (780)
$\varepsilon=10^{-6}$	$L_{\text{theo.}}$	0 (0)	9 (190)	12 (325)	17 (630)	25 (1326)
	$L_{\text{num.}}$	0 (0)	7 (120)	10 (231)	16 (561)	24 (1225)
$\varepsilon=10^{-9}$	$L_{\text{theo.}}$	0 (0)	11 (276)	15(496)	20 (861)	30 (1891)
	$L_{\text{num.}}$	0 (0)	9 (190)	13 (378)	18 (703)	28 (1653)
$\varepsilon=10^{-12}$	$L_{\text{theo.}}$	0 (0)	13 (378)	17(630)	24 (1225)	34 (2415)
	$L_{\text{num.}}$	0 (0)	12 (329)	15 (496)	21 (946)	32 (2145)

Table 1: Comparison between the number $L_{\text{theo.}}$ given by (21) to achieve an accuracy of 10^{-3}, 10^{-6}, 10^{-9} or 10^{-12} for five possible cell sizes and the number $L_{\text{num.}}$ obtained numerically by checking that the error remains below the prescribed level if $L_{\text{num.}}$ is decreased. The total number of quadrature points $(L+1)(2L+1)$ is also reported into brackets.

3.2 A new translation function for the propagative part

Expression (9) of the propagative part defined the translation function needed in (2). Using the quadrature defined in Section 3.1, it provides an expansion similar to a multipole expansion in the FMM of Rokhlin. The translation function $T(\hat{s},\vec{t}) = \frac{ik}{2\pi}\pi(\hat{s})e^{ik\vec{t}\cdot\hat{s}}$ needs in practice to be truncated to reduce the number of quadrature points on the unit sphere. Since $\pi(\hat{s})$ is discontinuous on the meridian circle $\hat{s}\cdot\hat{z}=0$, it is very likely that the convergence of the expansion of the translation function, in terms of spherical harmonics (17) will be slow, especially in the vicinity of the circular line of discontinuity. We give in Proposition 3.2 an alternative expression of the translation function to the one proposed in [11] to avoid this problem.

Proposition 3.2 *Let π be the characteristic function of the upper hemisphere (10) and Π^L be the orthogonal projector in $L^2(S^2)$ (17). We have*

$$T^L(\hat{s},\vec{t}) = \Pi^L\left(\frac{ik}{2\pi}e^{ik\hat{s}\cdot\vec{t}}\,\pi(\hat{s})\right)(\hat{s}) = 2ik\sum_{p=0}^{L}\sum_{m=-p}^{p}\left(\sum_{n=|m|}^{\infty} i^n j_n(kt)\,\gamma_{n,p}^m\overline{Y_n^m(\hat{t})}\right)Y_p^m(\hat{s}) \tag{25}$$

where the Y_n^m are the spherical harmonics (15)-(16) and the $\gamma_{n,p}^m$ are the coupling parameters:

$$\begin{cases} \gamma_{n,n}^m = \dfrac{1}{2}, \quad \gamma_{n,p}^m = \dfrac{1}{2}\sqrt{(2n+1)(2p+1)}\,\tilde{\gamma}_{n,p}^m \quad \text{when } n\neq p; \\ \tilde{\gamma}_{n,p}^m = \dfrac{\tilde{P}_p^{|m|}\sqrt{n^2-m^2}\tilde{P}_{n-1}^{|m|} - \tilde{P}_n^{|m|}\sqrt{p^2-m^2}\tilde{P}_{p-1}^{|m|}}{n(n+1)-p(p+1)}; \\ \text{with } \tilde{P}_{|m|+2k+1}^{|m|} := 0, \quad \tilde{P}_{-1}^{|m|} := 0, \quad \tilde{P}_{|m|+2k}^{|m|} := (-1)^{k+|m|}\beta_{k+|m|}\beta_k; \\ \beta_0 := 1, \quad \beta_k := \displaystyle\prod_{q=1}^{k}\sqrt{1-\frac{1}{2q}}. \end{cases} \tag{26}$$

Proof: We look for the expansion of the function $T : \hat{s} \mapsto \frac{ik}{2\pi}\pi(\hat{s})\,e^{ik\hat{s}\cdot\vec{t}}$ in terms of spherical harmonics. Using both the Jacobi Anger expansion and the addition Theorem

$$e^{ik\hat{s}\cdot\vec{t}} = \sum_{n=0}^{\infty} i^n j_n(kt)\,(2n+1)P_n(\hat{s}\cdot\hat{t}), \quad (2n+1)P_n(\hat{s}\cdot\hat{t}) = 4\pi\sum_{m=-n}^{m=n} Y_n^m(\hat{s})\overline{Y_n^m(\hat{t})},$$

it follows that

$$\pi(\hat{s})\, e^{ik\hat{s}\cdot\vec{t}} = 4\pi \sum_{n=0}^{\infty} i^n j_n(kt) \sum_{m=-n}^{n} (\pi(\hat{s}) Y_n^m(\hat{s}))\, \overline{Y_n^m(\hat{t})}. \tag{27}$$

The coordinate system (16) makes $\hat{s} \mapsto \pi(\hat{s})$ invariant by any rotation with respect to φ. Consequently $\pi(\hat{s})Y_n^m(\hat{s})$ is orthogonal to $Y_p^{m'}(\hat{s})$ when $m' \neq m$ and

$$\pi(\hat{s})Y_n^m(\hat{s}) = \sum_{p=|m|}^{\infty} \gamma_{n,p}^m Y_p^m(\hat{s}) \quad \text{with} \quad \gamma_{n,p}^m = \int_{S^2} \pi(\hat{s}) Y_n^m(\hat{s}) \overline{Y_p^m(\hat{s})}\, d\sigma(\hat{s}). \tag{28}$$

Plugging (28) into (27) and interchanging the order of summation, we obtain

$$\frac{2ik}{2\pi}\, \pi(\hat{s}) e^{ik\hat{s}\cdot\vec{t}} = 2ik \sum_{p=0}^{\infty} \sum_{m=-p}^{p} \left(\sum_{n=|m|}^{\infty} i^n j_n(kt) \gamma_{n,p}^m \overline{Y_n^m(\hat{t})} \right) Y_p^m(\hat{s})$$

$$\text{and} \quad \Pi^L \left(\frac{ik}{2\pi}\, \pi(\hat{s}) e^{ik\hat{s}\cdot\vec{t}} \right) = 2ik \sum_{p=0}^{L} \sum_{m=-p}^{p} \left(\sum_{n=|m|}^{\infty} i^n j_n(kt) \gamma_{n,p}^m \overline{Y_n^m(\hat{t})} \right) Y_p^m(\hat{s}).$$

The last point is the evaluation of the coupling coefficients $\gamma_{n,p}^m$. We use the definition of the spherical harmonics (15) to obtain

$$\gamma_{n,p}^m = 2\pi \frac{\sqrt{(2n+1)(2p+1)}\, \tilde{\gamma}_{n,p}^{|m|}}{4\pi} \text{ with } \tilde{\gamma}_{n,p}^{|m|} = \sqrt{\frac{(n-|m|)!}{(n+|m|)!}} \sqrt{\frac{(p-|m|)!}{(p+|m|)!}} \int_0^1 P_n^{|m|}(x) P_p^{|m|}(x)\, dx.$$

When $n = p$, we get ([8]) $\gamma_{p,p}^{|m|} = \frac{1}{2}(2p+1)\frac{(p-|m|)!}{(p+|m|)!}\left(\frac{1}{2}\int_{-1}^{1} |P_p^{|m|}(x)|^2 dx\right) = \frac{1}{2}$.

When $n \neq p$, $P_p^{|m|}(x)$ and $P_n^{|m|}(x)$ satisfy the following two differential equations

$$(a) \quad \Big((1-x^2)P_n^{|m|\,\prime}(x)\Big)' + n(n+1)P_n^{|m|}(x) - \frac{m^2}{1-x^2} P_n^{|m|}(x) = 0,$$

$$(b) \quad \Big((1-x^2)P_p^{|m|\,\prime}(x)\Big)' + p(p+1)P_p^{|m|}(x) - \frac{m^2}{1-x^2} P_p^{|m|}(x) = 0.$$

Multiplying (a) by $P_p^{|m|}(x)$, (b) by $P_n^{|m|}(x)$, integrating the difference of the two equalities over $[0,1]$ and performing two integrations by parts, we obtain

$$\int_0^1 P_n^{|m|}(x) P_p^{|m|}(x)\, dx = \frac{P_p^{|m|}(0) P_n^{|m|\prime}(0) - P_n^{|m|}(0) P_p^{|m|\prime}(0)}{n(n+1) - p(p+1)}.$$

Using the tilded "associated Legendre functions" $\tilde{P}_n^{|m|} := \tilde{P}_n^{|m|}(0) = \sqrt{\frac{(n-|m|)!}{(n+|m|)!}}\, P_n^{|m|}(0)$, we get

$$\gamma_{n,p}^m = \frac{1}{2}\sqrt{(2n+1)(2p+1)}\, \frac{\tilde{P}_p^{|m|} \tilde{P}_n^{|m|\prime} - \tilde{P}_n^{|m|} \tilde{P}_p^{|m|\prime}}{n(n+1) - p(p+1)}$$

and (26) follows from $\tilde{P}_\nu^{|m|\prime} = \sqrt{\nu^2 - m^2}\, \tilde{P}_{\nu-1}^{|m|}$ and the known values for $P_\nu^k(0)$ [1, 8.6.1]. ■

The advantage of this new expression of the translation function lies in its fast evaluation. In practice it is necessary to truncate expansion (25) to some integer N but it is possible to estimate the error introduced by this truncation.

Lemma 3.2 *The translation function (25) is numerically approximated by*

$$\Pi^L\left(\frac{ik}{2\pi}e^{ik\hat{s}\cdot\vec{t}}\pi(\hat{s})\right)(\hat{s}) \simeq 2ik\sum_{p=0}^{L}\sum_{m=-p}^{p}\left(\sum_{n=|m|}^{N} i^n j_n(kt)\gamma_{n,p}^m\overline{Y_n^m(\hat{t})}\right)Y_p^m(\hat{s}).$$

We define the induced error by

$$E_L^N(kt,\hat{t},\hat{s}) = 2ik\sum_{p=0}^{L}\sum_{m=-p}^{p}\left(\sum_{n=N+1}^{\infty} i^n j_n(kt)\gamma_{n,p}^m\overline{Y_n^m(\hat{t})}\right)Y_p^m(\hat{s}),$$

then E_L^N is uniformly bounded as

$$\sup_{\hat{s},\hat{t}} E_L^N(kt,\hat{t},\hat{s}) \le \frac{k}{2\pi}\,C_N^L\,\left(\frac{A_N(kt)+A_{N+1}(kt)}{2}\right)^{\frac{1}{2}},\ \textit{if } N>L+1 \tag{29}$$

with $C_N^L = \frac{4}{\pi}\,(2L+1)^{\frac{1}{4}}\,\frac{((N+\frac{1}{2})^2+(L+\frac{3}{2})^2)^{\frac{1}{2}}}{((N+\frac{1}{2})^2-(L+\frac{3}{2})^2)^{\frac{1}{4}}}$ *and* $A_N(v) = v^2 j_N(v)^2 - v^2 j_{N+1}(v)j_{N-1}(v)$.

Proof: First, we introduce $\delta_{n,p} = \sqrt{2n+1}\sqrt{2p+1}\,\max_{m=0,\dots,p}|\gamma_{n,p}^m|$ and we use

$$E_L^N(v,\hat{t},\hat{s}) \le 2k\sum_{p=0}^{L}\sum_{n=N+1}^{\infty}\frac{|j_n(v)|\,\delta_{n,p}}{\sqrt{(2n+1)(2p+1)}}\left(\sum_{m=-p}^{p}|Y_n^m(\hat{t})|^2\right)^{\frac{1}{2}}\left(\sum_{m=-p}^{p}|Y_n^m(\hat{s})|^2\right)^{\frac{1}{2}}.$$

Since $4\pi\sum_{m=-q}^{q}|Y_q^m(\hat{s})|^2 = 2q+1$, it follows that

$$\sup_{\hat{s},\hat{t}} E_L^N(v,\hat{t},\hat{s}) \le \frac{k}{2\pi}\sum_{n=N+1}^{\infty}|j_n(v)|\sum_{p=0}^{L}\delta_{n,p}. \tag{30}$$

Introducing the positive weight $\varpi_p = (2p+1)^{-\frac{1}{2}}$, the Cauchy-Schwartz inequality gives

$$\begin{aligned}\sum_{n=N+1}^{\infty}\sum_{p=0}^{L}|j_n(v)|\,\delta_{n,p} &\le \left(\sum_{n=N+1}^{\infty}\sum_{p=0}^{L}\frac{(\delta_{n,p})^2}{\varpi_p(2n+1)}\right)^{\frac{1}{2}}\left(\sum_{p=0}^{L}\varpi_p\sum_{n=N+1}^{\infty}(2n+1)j_n(v)^2\right)^{\frac{1}{2}}\\ &\le \left(\sum_{n=N+1}^{\infty}\sum_{p=0}^{L}\frac{(\delta_{n,p})^2}{\varpi_p(2n+1)}\right)^{\frac{1}{2}}\left(\sum_{p=0}^{L}\varpi_p\right)^{\frac{1}{2}}\left(\frac{A_N(v)+A_{N+1}(v)}{2}\right)^{\frac{1}{2}}.\end{aligned}$$

To bound δ_n^p, we start with the definition of the coupling parameters (26) and use the equality $|\tilde{P}_n^{|m|}(0)|^2 = |P_{n-|m|}(0)P_{n+|m|}(0)|$ with the bound $|P_p(0)| \le \sqrt{\frac{2}{\pi(p+\frac{1}{2})}}$. Then, after some tedious calculations, we obtain that

$$\text{when } N>L+1,\quad \delta_{n,p} \le \frac{2}{\pi}\,\frac{(2n+1)(2p+1)^{\frac{3}{4}}}{((n+\frac{1}{2})^2-(p+\frac{1}{2})^2)^{\frac{3}{4}}}\quad\text{and}\quad\sum_{p=0}^{L}\varpi_p \le \sqrt{2L+1}.$$

The remaining double series can be interpreted as a Riemann sum and the result is obtained since

$$\begin{aligned}&\sum_{n=N+1}^{\infty}\sum_{p=0}^{L}\frac{(\delta_{n,p})^2}{\varpi_p(2n+1)} \le \frac{16}{\pi^2}\int_{N+\frac{1}{2}}^{\infty}\int_0^{L+\frac{3}{2}}\frac{xy}{(x^2-y^2)^{\frac{3}{2}}}\,dxdy = \frac{16}{\pi^2}\int_{N+\frac{1}{2}}^{\infty}\int_0^{L+\frac{3}{2}}\mathrm{Div}(\frac{(x^2y,y^2x)}{(x^2-y^2)^{\frac{3}{2}}})\,dxdy\\ &= \frac{16}{\pi^2}\Big(\int_0^{L+\frac{3}{2}}\frac{(N+\frac{1}{2})^2y}{((N+\frac{1}{2})^2-y^2)^{\frac{3}{2}}}dy + \int_{N+\frac{1}{2}}^{\infty}\frac{(L+\frac{3}{2})^2x}{(x^2-(L+\frac{3}{2})^2)^{\frac{3}{2}}}dx\Big) = \frac{16}{\pi^2}\frac{(N+\frac{1}{2})^2+(L+\frac{3}{2})^2}{((N+\frac{1}{2})^2-(L+\frac{3}{2})^2)^{\frac{1}{2}}}.\end{aligned}$$

4 Numerical evaluation of the evanescent part of the Green's function

4.1 Efficient and accurate quadrature rule for the evanescent part

The linearization of the phase introduced in (14) leads to some major simplifications in the derivation of an efficient quadrature rule. Indeed, we use the quadrature defined for the static case $k = 0$ proposed in [30]. We consider now an angle $\varphi_w \in [0, 2\pi]$ and some $\hat{r}_w, \hat{z}_w \in d\hat{\Omega}$ with $\hat{\Omega}$ defined in (12) and shown in Figure 1. The aim is to design a quadrature rule to evaluate accurately the integral in the (φ, λ)-space

$$G_e(\vec{w}) = \frac{1}{2\pi} \int_0^\infty \int_0^{2\pi} e^{i(k\vec{w}\cdot\vec{s}(\varphi) + \lambda\vec{w}\cdot\vec{t}(\varphi))} d\varphi d\lambda \quad \text{with}$$

$$\vec{s}(\varphi) = \begin{bmatrix} \cos\varphi \\ \sin\varphi \\ 0 \end{bmatrix}, \qquad \vec{t}(\varphi) = \begin{bmatrix} \sin\varphi \\ -\cos\varphi \\ i \end{bmatrix}, \qquad \vec{w} = \begin{bmatrix} r_w \cos\varphi_w \\ r_w \sin\varphi_w \\ z_w \end{bmatrix}. \tag{31}$$

If we consider the angular integration over φ independently from the integration over λ, the optimal choice is to use equidistributed angles (to perform the interpolation with the FFT). However, we will show that the optimal choice, in the sense of the smallest total number of points for an accurate integration in the (φ, λ)-space, is to consider a different quadrature over φ for each value of λ. We define the optimal choice for the radial integration over λ in Proposition 4.1.

Proposition 4.1 *Let ε_1, ε_2 be two small positive numbers. Assume that there exists a P-point quadrature rule with positive weights $(\tilde{\lambda}_p, \varpi_p)_{p=1,\dots,P}$ such that*

$$\max_{\xi\in\hat{\Omega}} \left| \sum_{p=1}^{P} \varpi_p e^{-\tilde{\lambda}_p \xi} - \frac{1}{\xi} \right| \leq \frac{\varepsilon_1}{4\sqrt{3}}. \tag{32}$$

For each quadrature point $\tilde{\lambda}_p$, define $Q_{p,kd} = Q(\tilde{\lambda}_p, kd, \varepsilon_2)$ as the smallest integer such that

$$Q_{p,kd} \geq \tau_p + 1 \text{ and } \sum_{k=Q_{p,kd}+1}^{\infty} J_k(\tau_p) \leq \frac{\varepsilon_2}{2\sqrt{19}}, \quad \text{with } \tau_p = 4\sqrt{2}\sqrt{(kd)^2 + \tilde{\lambda}_p^2}. \tag{33}$$

For each $\tilde{\lambda}_p$, define the $Q_{p,kd}$ equidistributed angles $\varphi_{p,q} = \frac{2\pi q}{Q_{p,kd}}$, $0 \leq q \leq Q_{p,kd} - 1$. Then, the approximation of $G_e(\vec{w})$ with the previously defined quadrature rule

$$G_e^P(\vec{w}) = \frac{1}{d} \sum_{p=1}^{P} \sum_{q=1}^{Q_{p,kd}} \frac{\varpi_p}{Q_{p,kd}} e^{i(kd\vec{s}(\varphi_{p,q}) + \tilde{\lambda}_p \vec{t}(\varphi_{p,q}))\cdot\frac{\vec{w}}{d}}$$

satisfies

$$\max_{\vec{w}\in\Omega_d} |\vec{w}| \left| G_e^P(\vec{w}) - G_e(\vec{w}) \right| \leq \varepsilon_1 + \varepsilon_2 + \frac{\varepsilon_1\varepsilon_2}{\sqrt{19}}. \tag{34}$$

It is possible in practice to define a quadrature satisfying (32). It is simply a quadrature accurate for integrating $e^{-\lambda\xi}$ for any ξ, i.e. a quadrature for the static case. It results that the radial integration is performed with the quadrature points and weights given by Yarvin and

Rokhlin; in [30], 41 laws are given to achieve various levels of accuracy ranging between 10^{-2} and 10^{-14}. In addition, we prove in the following that condition (33) is sufficient to ensure

$$\sup_\varphi \left| J_0(t) - \frac{1}{Q}\sum_{q=0}^{Q-1} e^{it\cos(\frac{2\pi q}{Q}-\varphi)} \right| < \frac{\varepsilon_2}{\sqrt{19}}.$$

In practice, an easy way to determine numerically Q consists in looking for the smallest $Q > \tau_p = t$ such that

$$\left| J_0(t) - \frac{1}{Q}\sum_{q=0}^{Q-1} e^{it\cos(\frac{2\pi q}{Q})} \right| < \frac{\varepsilon_2}{\sqrt{19}} \quad (Q \text{ odd}) \quad \text{or} \quad \left| J_0(t) - \frac{1}{Q}\sum_{q=0}^{Q-1} e^{it\sin(\frac{2\pi q}{Q})} \right| < \frac{\varepsilon_2}{\sqrt{19}} \quad (Q \text{ even}).$$

Finally, Proposition 4.1 provides enough information to define in practice a quadrature rule while keeping the error below a prescribed level.

Proof: We start from the definition of the error induced by the quadrature rule

$$\begin{aligned} e^P(\vec{w}) &= |\vec{w}| \left| G_e(\vec{w}) - G_e^P(\vec{w}) \right| \\ &= \frac{|\vec{w}|}{2\pi} \left| \int_0^\infty \int_0^{2\pi} e^{i(k\vec{w}\cdot\vec{s}(\varphi)+\lambda\vec{w}\cdot\vec{t}(\varphi))} d\varphi d\lambda \; - \; \fint_0^\infty \fint_0^{2\pi} e^{i(k\vec{w}\cdot\vec{s}(\varphi)+\lambda\vec{w}\cdot\vec{t}(\varphi))} d\varphi d\lambda \right|. \end{aligned}$$

Introducing the function $f(\lambda,\phi) = e^{i(k\vec{w}\cdot\vec{s}(\varphi)+\lambda\vec{w}\cdot\vec{t}(\varphi))}$, and using the triangular inequality, we have

$$\left| \int_0^\infty \int_0^{2\pi} f(\lambda,\varphi) d\varphi d\lambda \; - \; \fint_0^\infty \fint_0^{2\pi} f(\lambda,\varphi) d\varphi d\lambda \right| \leq$$
$$\int_0^{2\pi} \left| \int_0^\infty f(\lambda,\varphi) d\lambda - \fint_0^\infty f(\lambda,\varphi) d\lambda \right| d\varphi + \fint_0^\infty \left| \int_0^{2\pi} f(\lambda,\varphi) d\varphi - \fint_0^{2\pi} f(\lambda,\varphi) d\varphi \right| d\lambda.$$

We consider first the term

$$\begin{aligned} \left| \int_0^\infty f(\lambda,\varphi) d\lambda - \fint_0^\infty f(\lambda,\varphi) d\lambda \right| &= \frac{1}{d} \left| \int_0^\infty e^{i(\tilde{\lambda}\frac{\vec{w}}{d}\cdot\vec{t}(\varphi))} d\tilde{\lambda} - \fint_0^\infty e^{i(\tilde{\lambda}\frac{\vec{w}}{d}\cdot\vec{t}(\varphi))} d\tilde{\lambda} \right| \left| e^{ik\vec{w}\cdot\vec{s}(\varphi)} \right| \\ &= \frac{1}{d} \left| \frac{1}{\xi(\varphi,\vec{w})} - \sum_p \varpi_p e^{-\tilde{\lambda}_p \xi(\varphi,\vec{w})} \right| \end{aligned}$$

with $\xi(\varphi,\vec{w}) = z_w/d + i r_w \sin(\varphi_w - \varphi)/d$. We have made the assumption that $(r_w, z_w) \in d\hat{\Omega}$ such that $\xi(\varphi,\vec{w}) \in \hat{\Omega}$ and we use (32) to obtain

$$\left| \int_0^\infty f(\lambda,\varphi) d\lambda - \fint_0^\infty f(\lambda,\varphi) d\lambda \right| \leq \frac{\varepsilon_1}{4\sqrt{3}d}.$$

Finally, since $|\vec{w}| \leq 4\sqrt{3}d$, we obtain

$$\frac{|\vec{w}|}{2\pi d} \int_0^{2\pi} \left| \int_0^\infty f(\lambda,\varphi) d\lambda - \fint_0^\infty f(\lambda,\varphi) d\lambda \right| d\varphi \leq \varepsilon_1.$$

We turn now to the second term; introducing the variables $t_p = \sqrt{k^2 d^2 + \tilde{\lambda}_p^2}$, $kd = t_p \cos\psi_p$ with $\tilde{\lambda}_p = t_p \sin\psi_p$, (see (13)), this term is given by

$$\frac{1}{2\pi} \left| \left(\int_0^{2\pi} - \fint_0^{2\pi} \right) \left(e^{i(k\vec{w}\cdot\vec{s}(\varphi) + \tilde{\lambda}\frac{\vec{w}}{d}\cdot\vec{t}(\varphi))} \right) \right| = e^{-\tilde{\lambda}_p \frac{z_w}{d}} \left| J_0(t_p \frac{r_w}{d}) - \frac{1}{Q_{p,kd}} \sum_{q=1}^{Q_{p,kd}} e^{it_p \frac{r_w}{d}\cos(\varphi_{p,q} - \varphi_w - \psi_p)} \right|.$$

Having in mind the definition of Bessel functions (8) and introducing $J_0^Q(v,\varphi)$, the sum obtained using a Q-point quadrature rule, we obtain

$$\left|\frac{1}{2\pi}\left(\int_0^{2\pi} - \fint_0^{2\pi}\right)\left(e^{i(k\vec{w}\cdot\vec{s}(\varphi)+\tilde{\lambda}\frac{\vec{w}}{d}\cdot\vec{t}(\varphi))}\right)\right| = e^{-\tilde{\lambda}_p\frac{z_w}{d}}\left|J_0(t_p\frac{r_w}{d}) - J_0^{Q_{p,kd}}(t_p\frac{r_w}{d},\varphi_w+\psi_p)\right|,$$

where $J_0^Q(v,\varphi) = \dfrac{1}{Q}\displaystyle\sum_{q=1}^{Q} e^{iv\cos(\varphi_q^Q-\varphi)}$ and $\varphi_q^Q = \dfrac{2\pi q}{Q}$. Using the 2-D Jacobi-Anger expansion [8], we get

$$J_0(v) - J_0^Q(v,\varphi) = -2\sum_{\ell=1}^{\infty} i^\ell J_\ell(v)\left(\frac{1}{Q}\sum_{q=1}^{Q}\cos(\ell(\varphi_q^Q-\varphi))\right) = 2\sum_{q=1}^{\infty} i^{qQ}J_{qQ}(v)\cos(qQ\varphi)$$

and consequently

$$\max_{\varphi}\left|J_0(v) - J_0^Q(v,\varphi)\right| \le 2\sum_{q=1}^{\infty}|J_{qQ}(v)| \le 2\sum_{q\ge Q}^{\infty}|J_q(v)|.$$

Let's now consider the behavior of $f : v \mapsto 2\sum_{q\ge Q}^{\infty}|J_q(v)|$ on $[0, Q-1]$:

$$\frac{d}{dv}f(v) = \sum_{q\ge Q}^{\infty}(J_{q-1}(v) - J_{q+1}(v)) = J_{Q-1}(v) + J_Q(v) > 0.$$

Since $J_q(v)$ is positive on this interval, f increases on $[0, Q-1]$. In addition, we have made the assumption that $Q_{p,kd} \ge \tau_p + 1$ and $\sum_{k=Q_{p,kd}+1}^{\infty} J_k(\tau_p) \le \frac{\varepsilon_2}{2\sqrt{19}}$ with $\tau_p = 4\sqrt{2}t_p$. Since v is at most equal to τ_p (defined in (33)), the error is uniformly bounded by $\frac{\varepsilon_2}{\sqrt{19}}$ and the second term is bounded by

$$\frac{|\vec{w}|}{2\pi d}\fint_0^{\infty}\left|\int_0^{2\pi} e^{i(k\vec{w}\cdot\vec{s}(\varphi)+\tilde{\lambda}\frac{\vec{w}}{d}\cdot\vec{t}(\varphi))}d\varphi - \fint_0^{2\pi} e^{i(k\vec{w}\cdot\vec{s}(\varphi)+\tilde{\lambda}\frac{\vec{w}}{d}\cdot\vec{t}(\varphi))}d\varphi\right| d\lambda \quad\le\quad \varepsilon_2\frac{|\vec{w}|}{\sqrt{19}d}\fint_0^{\infty} e^{-\tilde{\lambda}_p\frac{z_w}{d}}d\tilde{\lambda}.$$

Using Hypothesis (32) on the quadrature for the radial integration, we get

$$\frac{|\vec{w}|}{2\pi d}\fint_0^{\infty}\left|\int_0^{2\pi} e^{i(k\vec{w}\cdot\vec{s}(\varphi)+\tilde{\lambda}\frac{\vec{w}}{d}\cdot\vec{t}(\varphi))}d\varphi - \fint_0^{2\pi} e^{i(k\vec{w}\cdot\vec{s}(\varphi)+\tilde{\lambda}\frac{\vec{w}}{d}\cdot\vec{t}(\varphi))}d\varphi\right| d\lambda \le \varepsilon_2\frac{|\vec{w}|}{\sqrt{19}d}\int_0^{\infty} e^{-\tilde{\lambda}_p\frac{z_w}{d}} + \frac{\varepsilon_1\varepsilon_2}{4\sqrt{3}}\frac{|\vec{w}|}{\sqrt{19}d}.$$

Since the maximum of $\frac{|\vec{w}|}{z_w}$ on Ω_d is reached when $z_w = d$ and $r_w = 3\sqrt{2}d$ with value $\sqrt{19}$, we have

$$\frac{|\vec{w}|}{2\pi d}\fint_0^{\infty}\left|\int_0^{2\pi} e^{i(k\vec{w}\cdot\vec{s}(\varphi)+\tilde{\lambda}\frac{\vec{w}}{d}\cdot\vec{t}(\varphi))}d\varphi - \fint_0^{2\pi} e^{i(k\vec{w}\cdot\vec{s}(\varphi)+\tilde{\lambda}\frac{\vec{w}}{d}\cdot\vec{t}(\varphi))}d\varphi\right| d\lambda \quad\le \varepsilon_2 + \tfrac{\varepsilon_1\varepsilon_2}{\sqrt{19}}. \ \blacksquare$$

4.2 Filtering the translation function of the evanescent part

The quadrature proposed in Proposition 4.1 is not optimal for the `PWFMM` since it does not use the decomposition of the vector $\vec{w}$ as $\vec{w} = \vec{t} + \vec{v}$. This property is used to reduce the number of angles. Actually, the aim is to evaluate

$$\left\{\begin{array}{l} G_e(\vec{t}+\vec{v}) = \dfrac{1}{2\pi}\displaystyle\int_0^{\infty}\int_0^{2\pi} e^{i(k\vec{s}(\varphi)+\lambda\vec{t}(\varphi))\cdot\vec{t}}\, e^{i(k\vec{s}(\varphi)+\lambda\vec{t}(\varphi))\cdot\vec{v}}\, d\varphi d\lambda \\ \text{with} \quad \left\{\begin{array}{c} \vec{t} = d(i\hat{x}+j\hat{y}+m\hat{z}),\ i,j,m \text{ relative integers;} \\ 3 \ge m \ge |i|,\ |j| \text{ and } i^2+j^2+m^2 > 3; \vec{v} \in d\hat{B} = d\,[-1,1]^3\,. \end{array}\right. \end{array}\right. \tag{35}$$

Similarly to the approach used in Lemma 3.1, the idea is to filter out the Fourier modes of the plane wave expansion that do not contribute much to the value of the integral.

Proposition 4.2 *Let ε_1, ε_2 be two small positive numbers. Assume that there exists a P-point quadrature rule with positive weights $(\tilde{\lambda}_p, \varpi_p)_{p=1,,\dots,P}$ such that Condition (32) holds. For each $\tilde{\lambda}_p$, define $Q_{p,kd} = Q(\tilde{\lambda}_p, kd, \varepsilon_2) = 2L_p + 1$ such that*

$$L_p \geq \tau_p, \ \left(2\sum_{k=L_p+1}^{\infty} J_k^2(\sqrt{2}\tau_p)\right)^{\frac{1}{2}} + 2\sum_{k=L_p+1}^{\infty} J_k(\sqrt{2}\tau_p) \leq \frac{\varepsilon_2}{\sqrt{19}} \text{ and } \tau_p = \sqrt{(kd)^2 + \tilde{\lambda}_p^2}. \quad (36)$$

For each $\tilde{\lambda}_p$, the angular integration is performed with $Q_{p,kd}$ equidistributed points $\varphi_{p,q} = \frac{2\pi q}{Q_{p,kd}}$, $0 \leq q \leq Q_{p,kd} - 1$. We define $T^L(\vec{t}; \lambda, \varphi)$ the filtered translation function

$$T^L(\vec{t}; \lambda, \varphi) = e^{-\tilde{\lambda}\frac{z_t}{d}} \sum_{q=0}^{L} \varepsilon_q i^q J_q(\tau \frac{r_t}{d}) \cos(q(\varphi - \varphi_t - \psi_\lambda)) \quad (37)$$

with $\tau = \sqrt{\tilde{\lambda}^2 + k^2 d^2}$, $kd = \tau \cos\psi_\lambda$, $\tilde{\lambda} = \tau \sin\psi_\lambda$. Then, for $\vec{t}$ and $\vec{v}$ satisfying (35) the filtered evanescent part G_e^P with the previously defined quadrature rule

$$G_e^P(\vec{t}, \vec{v}) = \frac{1}{d}\sum_{p=1}^{P}\sum_{q=1}^{Q_{p,kd}} \frac{\varpi_p}{Q_{p,kd}} T^{L_p}(\vec{t}; \tilde{\lambda}_p, \varphi_{p,q}) \, e^{i(kd\vec{s}(\varphi_{p,q}) + \tilde{\lambda}_p \vec{t}(\varphi_{p,q}))\cdot\frac{\vec{v}}{d}} \quad (38)$$

satisfies the error estimate

$$\max_{\vec{t}+\vec{v}\in\Omega_d} |\vec{t}+\vec{v}| \left|G_e^P(\vec{t}, \vec{v}) - G_e(\vec{t}+\vec{v})\right| \leq \varepsilon_1 + \varepsilon_2 + \frac{\varepsilon_1\varepsilon_2}{\sqrt{19}}. \quad (39)$$

The use of the filtered translation function permits to reduce the number of points in the quadrature. Since the filtered translation function is defined for λ given, only the number of angles φ is reduced (roughly by a factor 2). A similar filtering of the translation function in λ would be efficient but it would require to choose an adequate orthogonal basis; this choice is quite difficult since the function to filter mixes the variables λ and φ. To illustrate the relevance of this filtering, we report in Table 2 the total number of quadrature points Q (with $Q = \sum_{p=1}^{P} Q_{p,kd}$) determined by (32) and (36) to achieve four levels of accuracy: 10^{-3}, 10^{-6}, 10^{-9} or 10^{-12} and for five cell sizes. The number of points Q is seen to increase slightly with the cell size. In addition, similarly to the numerical experiments for the propagative part, we sample the faces of a cell with 600 vectors $\vec{v}$ and compute the error (39) for all the possible vectors $\vec{t}$. These numerical experiments corroborate that the errors observed numerically are always smaller than the accuracies prescribed, by a factor roughly equal to 10 whatever the frequency is.

Proof: The proof follows the same lines as that of Proposition 4.1. We decompose the error into

$$\begin{aligned} e^P(\vec{w}) &= |\vec{w}| \left|G_e(\vec{w}) - G_e^P(\vec{w})\right| \\ &\leq \frac{|\vec{w}|}{2\pi}\int_0^{2\pi}\left|\int_0^{\infty} f(\lambda,\varphi)d\lambda - \oint_0^{\infty} f(\lambda,\varphi)d\lambda\right| d\varphi + \frac{|\vec{w}|}{2\pi}\oint_0^{\infty}\left|\int_0^{2\pi} f(\lambda,\varphi)d\varphi - \oint_0^{2\pi} f^L(\lambda,\varphi)d\varphi\right| d\lambda \end{aligned}$$

where we have introduced the function $f(\lambda,\varphi) = e^{i(k\vec{w}\cdot\vec{s}(\varphi) + \lambda\vec{w}\cdot\vec{t}(\varphi))}$ and the filtered function $f^L(\lambda,\varphi) = \Pi_L\left(e^{i(k\vec{w}\cdot\vec{s}(\varphi) + \lambda\vec{w}\cdot\vec{t}(\varphi))}\right)$. Since the filtering concerns only the variable φ, the first

		Q				
	P	$d=0$	$d=\lambda/8$	$d=\lambda/4$	$d=\lambda/2$	$d=\lambda$
$e^P=10^{-3}$	12	368 4×10^{-4}	380 1.3×10^{-4}	396 1.2×10^{-4}	444 1.18×10^{-4}	556 1.14×10^{-4}
$e^P=10^{-6}$	20	992 2.08×10^{-7}	1 020 2.07×10^{-7}	1 056 2.06×10^{-7}	1 112 2.02×10^{-7}	1 340 1.9×10^{-7}
$e^P=10^{-9}$	29	2 008 2.04×10^{-10}	2 048 2.04×10^{-10}	2 076 2.03×10^{-10}	2 212 1.99×10^{-10}	2 412 1.8×10^{-10}
$e^P=10^{-12}$	38	3 384 1.6×10^{-13}	3 424 1.6×10^{-13}	3 496 1.59×10^{-13}	3 628 1.57×10^{-13}	3 908 1.46×10^{-13}

Table 2: Total number of quadrature points Q (with $Q=\sum_{p=1}^{P}Q_{p,kd}$) determined by (32) and (36) to achieve four levels of accuracy: $e^P=10^{-3}$, 10^{-6}, 10^{-9} or 10^{-12}, for five cell sizes. The second row for each accuracy reports the error (39) obtained with this value of Q.

estimate remains unchanged compared to the previous proof, i.e.

$$\frac{|\vec{w}|}{2\pi}\int_0^{2\pi}\left|\int_0^{\infty}f(\lambda,\varphi)d\lambda-\fint_0^{\infty}f(\lambda,\varphi)d\lambda\right|d\varphi \quad=\quad \frac{|\vec{w}|}{d}\left|\frac{1}{\xi(\varphi,\vec{w})}-\sum_p\varpi_p e^{-\tilde{\lambda}_p\xi(\varphi,\vec{w})}\right|\le\frac{|\vec{w}|\,\varepsilon_1}{4\sqrt{3}d}\le\varepsilon_1$$

with $\xi(\varphi,\vec{w})=z_w/d+ir_w\sin(\varphi_w-\varphi)/d$. The only difference when the filtered translation function is introduced lies on the treatment of the second term. Introducing the variables $\tau=\sqrt{k^2d^2+\tilde{\lambda}^2}$, $kd=\tau\cos\psi_\lambda$ and $\tilde{\lambda}=\tau\sin\psi_\lambda$, the second term reads (see (13))

$$\begin{aligned}&\frac{1}{2\pi}\left|\int_0^{2\pi}e^{i(k\vec{w}\cdot\vec{s}(\varphi)+\tilde{\lambda}\frac{\vec{w}}{d}\cdot\vec{t}(\varphi))}d\varphi-\fint_0^{2\pi}\Pi_L\Big(e^{i(k\vec{w}\cdot\vec{s}(\varphi)+\tilde{\lambda}\frac{\vec{w}}{d}\cdot\vec{t}(\varphi))}\Big)d\varphi\right|\\&\qquad=e^{-\tilde{\lambda}\frac{z_w}{d}}\left|J_0(\tau\frac{r_w}{d})-\frac{1}{2\pi}\fint_0^{2\pi}\Pi_L\Big(e^{i\frac{r_t}{d}\tau\cos(\psi_\lambda-\varphi+\varphi_t)}\Big)e^{i\frac{r_v}{d}\tau\cos(\psi_\lambda-\varphi+\varphi_v)}d\varphi\right|.\end{aligned}$$

We remark that Lemma 3.1 remains true if the unit sphere is replaced by $[0;2\pi]$; then, the error

$$\varepsilon^L=\frac{1}{2\pi}\int_0^{2\pi}T(\varphi)E(\varphi)-\frac{1}{2\pi}\fint_0^{2\pi}\Pi_LT(\varphi)E(\varphi)$$

satisfies the bound $|\varepsilon^L|\le\|T\|_2\left(\varepsilon_\infty^{L+1}+\varepsilon_2^L\right)$ with $\|T\|_2=\left(\frac{1}{2\pi}\int_0^{2\pi}|T(\varphi)|^2\right)^{\frac{1}{2}}$,

$$\varepsilon_\infty^L=\sup_{\varphi\in[0;2\pi]}|E(\varphi)-\Pi_LE(\varphi)| \quad\text{and}\quad \varepsilon_2^L=\left(\frac{1}{2\pi}\int_0^{2\pi}|E(\varphi)-\Pi_LE(\varphi)|^2\right)^{\frac{1}{2}}.$$

Defining $T(\varphi)=e^{i\frac{r_t}{d}\tau\cos(\psi_\lambda-\varphi+\varphi_t)}$ ($\|T\|_2=1$) and $E(\varphi)=e^{i\frac{r_v}{d}\tau\cos(\psi_\lambda-\varphi+\varphi_v)}$, the filtered translation function is calculated using Jacobi-Anger expansion

$$\Pi_LT(\varphi)=\sum_{q=0}^{L}\varepsilon_q i^qJ_q(\tau\frac{r_t}{d})\cos\Big(q(\varphi-\varphi_t-\psi_\lambda)\Big).$$

The errors ε_∞^L and ε_2^L are easily derived:

$$\varepsilon_\infty^L\le\left|2\sum_{q=L+1}^{\infty}J_q(t_p\frac{r_v}{d})\right| \quad\text{and}\quad \varepsilon_2^L\le\left|2\sum_{q=L+1}^{\infty}J_q^2(t_p\frac{r_v}{d})\right|^{1/2}.$$

Now using that $r_v \leq \sqrt{2}d$ and assumption (36), we conclude that $|\varepsilon^L| \leq \left(\varepsilon_\infty^{L+1} + \varepsilon_2^L\right) \leq \dfrac{\varepsilon_2}{\sqrt{19}}$. Finally, $\dfrac{|\vec{w}|}{2\pi}\displaystyle\int_0^\infty \left| \int_0^{2\pi} f(\lambda,\varphi)d\varphi - \int_0^{2\pi} f^L(\lambda,\varphi)d\varphi \right| d\lambda \leq \dfrac{\varepsilon_2}{\sqrt{19}}|\vec{w}| \displaystyle\int_0^\infty e^{-\tilde{\lambda}\frac{z_w}{d}} d\lambda \leq \varepsilon_2 + \dfrac{\varepsilon_1\varepsilon_2}{\sqrt{19}}$ and the result follows. ■

4.3 Interpolation of the evanescent part

The third ingredient listed in the introduction is the definition of a fast algorithm to perform the interpolation. Thus, some additional factorizations of the computations are obtained since the contributions at level-ℓ are used to evaluate the contributions at level-$(\ell-1)$. Let x_s be a point in a cell b of the octree; assume b is one of the eight children of the parent cell B; let $\vec{v}$ be the vector $x_s - c_B$, where c_B is the center of the cell B; The practical problem is to deduce

$$E(\vec{v};\lambda,\varphi) = e^{i(k\hat{s}(\varphi)+\lambda\hat{t}(\varphi))\cdot\vec{v}}$$

for any couple (λ,φ) of the quadrature defined at level-$(\ell-1)$, from the values $E(\vec{v};\lambda,\varphi)$ evaluated for the quadrature defined at level-ℓ. Following the results presented in §4.1 and §4.2, the quadrature points at level-ℓ (cell of size d) and at level-$(\ell-1)$ (parent cell of size $2d$) are defined by

$$\mathcal{C}_\ell^{quad} = \left\{ \left(\frac{\tilde{\lambda}_p}{d}, \varphi_q^{Q_{p,kd}} \right), \begin{array}{l} 1 \leq p \leq P, \\ 1 \leq q \leq Q_{p,kd} \end{array} \right\}; \quad \mathcal{C}_{\ell-1}^{quad} = \left\{ \left(\frac{\tilde{\lambda}_p}{2d}, \varphi_q^{Q_{p,2kd}} \right), \begin{array}{l} 1 \leq p \leq P, \\ 1 \leq q \leq Q_{p,2kd} \end{array} \right\}.$$

The number of points in the quadrature with respect to λ is constant (equal to P) since it is defined for the static case. But the quadrature points and weights depend on the level (i.e. the cell size d). Assuming that the $\tilde{\lambda}_p$ are ordered by increasing values, the maximum value is achieved for $p = P$, i.e. $\tilde{\lambda}_P$. On the other hand, the quadrature with respect to φ is composed of equidistributed points. Since the optimal quadrature is obtained by defining a different quadrature for each $\tilde{\lambda}_p$ $(p = 1, ..., P)$, the interpolation must solve two coupled problems: (i) how to link the non-uniform repartition of angles φ? (ii) how to perform the interpolation with respect to λ?

Interpolation with the FFT. Since the angles φ are equidistributed, the FFT is an appropriate tool to perform the interpolation. But we have to take into account that a different quadrature with respect to φ is defined for each $\tilde{\lambda}_p$. We denote by $Q = Q_{P,2kd}$ the maximum number of angles in the finest discretization with respect to φ (i.e. when $\tilde{\lambda}_p$ is equal to $\tilde{\lambda}_P$ and in the parent box). The idea is then to perform the interpolation independently for each $\tilde{\lambda}_p$. Algorithm 1 presents the three main steps to perform the interpolation. For each $\tilde{\lambda}_p$, **Step 1** consists in interpolating $E : \varphi \to E(\vec{v};\lambda,\varphi)$ to a uniform grid with Q points. Then, in **Step 2** the interpolation is performed with respect to λ for the Q angles φ. Finally for each $\tilde{\lambda}_p$, **Step 3** is the transpose of **Step 1** to go back on a grid with $Q_{p,2kd}$ angles. Now, assuming that the interpolator with respect to λ is independent from the value of φ, it is more efficient to stay in the Fourier space to perform the interpolation with respect to λ (see Algorithm 2).

Interpolation with respect to λ. **Step 2** of Algorithm 2 requires the definition of an accurate interpolator with respect to λ. To make its derivation clear, we decompose the problem into the following simpler steps:
Step 2a: Since the first term of the product $E(\vec{v};\lambda,\varphi) = e^{ik\hat{s}(\varphi)\cdot\vec{v}}\, e^{i\lambda\hat{t}(\varphi)\cdot\vec{v}}$ is independent of λ, we consider only $\tilde{E}(\vec{v},\lambda,\varphi) = e^{i\lambda\hat{t}(\varphi)\cdot\vec{v}}$ (independent of the wavenumber). The problem reduces

Algorithm 1 *Naive interpolation using the FFT.*

- **Step 1**: For each $p = 1, \dots P$
  1. `FFT` (of size $Q_{p,kd}$) of $e_q : q \mapsto E(\vec{v}; \frac{\tilde{\lambda}_p}{d}, \varphi_q^{Q_{p,kd}})$ to compute the Fourier coefficients $\hat{e}_m$, $|m| \leq \frac{Q_{p,kd}}{2}$
  2. Complete $\hat{e}_m$ for $[m[= \frac{Q_{p,kd}}{2} + 1, \dots, \frac{Q}{2}$ by adding zeros for the missing modes
  3. Inverse `FFT` (of size Q) to obtain the interpolated values of $E(\vec{v}; \frac{\tilde{\lambda}_p}{d}, \varphi)$ at points φ_q^Q
- **Step 2**: For each $q = 1, \dots Q$, for each $p = 1, \dots P$, perform the interpolation with respect to λ of the values of $E(\vec{v}; \frac{\tilde{\lambda}_p}{2d}, \varphi_q^Q)$ from the values of $E(\vec{v}; \frac{\tilde{\lambda}_p}{d}, \varphi_q^Q)$ (see steps 2a-d in the text)
- **Step 3**: For each $p = 1, \dots P$
  1. Compute the Fourier coefficients via an `FFT` of length Q of $e_q : q \mapsto E(\vec{v}; \frac{\tilde{\lambda}_p}{2d}, \varphi_q^Q)$
  2. Discard the modes larger than $\frac{Q_{p,2kd}}{2} + 1$
  3. Inverse `FFT` (of size $Q_{p,2kd}$) to obtain the interpolated values of $E(\vec{v}; \frac{\tilde{\lambda}_p}{2d}, \varphi)$ at points $\varphi_q^{Q_{p,2kd}}$

Algorithm 2 *More-efficient interpolation using the FFT.*

- **Step 1**: For each $p = 1, \dots P$
  1. `FFT` (of size $Q_{p,kd}$) of $e_q : q \mapsto E(\vec{v}; \frac{\tilde{\lambda}_p}{d}, \varphi_q^{Q_{p,kd}})$ to compute the Fourier coefficients $\hat{e}_m$, $|m| \leq \frac{Q_{p,kd}}{2}$
  2. Complete $\hat{e}_m$ for $[m[= \frac{Q_{p,kd}}{2} + 1, \dots, \frac{Q}{2}$ by adding zeros for the missing modes
- **Step 2**: For each $m = -\frac{Q}{2}, \frac{Q}{2}$, for each $p = 1, \dots P$, perform the interpolation with respect to λ of the values of $\hat{e}_m(\vec{v}; \frac{\tilde{\lambda}_p}{2d})$ from the values of $\hat{e}_m(\vec{v}; \frac{\tilde{\lambda}_p}{d})$ (see steps 2a-d in the text)
- **Step 3**: For $p = 1, \dots P$
  1. Discard the modes larger than $\frac{Q_{p,2kd}}{2} + 1$ in $\hat{e}_m(\vec{v}; \frac{\tilde{\lambda}_p}{2d})$
  2. Inverse `FFT` (of size $Q_{p,2kd}$) to obtain the interpolated values of $E(\vec{v}; \frac{\tilde{\lambda}_p}{2d}, \varphi)$ at points $\varphi_q^{Q_{p,2kd}}$

.

now to: knowing the values of $\tilde{E}$ at level-ℓ (child cell of size d), deduce the values of $\tilde{E}$ at level-

$(\ell-1)$ (parent cell of size $2d$).
Step 2b: If (r_v, φ_v, z_v) are the cylindrical coordinates of $\vec{v}$, we have

$$\hat{t}(\varphi)\cdot\frac{\vec{v}}{d} = \frac{r_v}{d}\sin(\varphi-\varphi_v) + i\frac{z_v}{d} = \zeta \in \mathbb{C}$$

and the function to be interpolated is $\tilde{E} \ : \ \tilde{\lambda} \mapsto e^{i\zeta\tilde{\lambda}}$ with ζ a function of $\vec{v}$. Since we choose to interpolate the fields of the small cells *ante* the multiplication with the phase shift (induced by the change of center of the cells), we have

$$\left|\frac{r_v}{d}\sin(\varphi-\varphi_v)\right| \leq \frac{\sqrt{2}}{2}, \left|\frac{z}{d}\right| \leq \frac{1}{2} \text{ and } \zeta \in \hat{C} = \left\{\zeta\in\mathbb{C}, -\frac{\sqrt{2}}{2} \leq \Re\zeta \leq \frac{\sqrt{2}}{2}, -\frac{1}{2} \leq \Im\zeta \leq \frac{1}{2}\right\}.$$

Step 2a is now equivalent to: compute for all ζ in $\hat{C}$, the values of $\tilde{E}(\tilde{\lambda}) = e^{i\tilde{\lambda}\zeta}$ at points $\frac{\tilde{\lambda}_p}{2}$ from the values of $\tilde{E}(\tilde{\lambda})$ at points $\tilde{\lambda}_p$ with $p = 1, \dots P$.
Step 2c: For a fixed value of q $(1 \leq q \leq P)$, we introduce $\kappa_p^q = \tilde{\lambda}_p - \frac{\tilde{\lambda}_q}{2}$ and **Step 2b** is equivalent to find the vector $\mathbb{M}^{(q)}$ of size P such that

$$J_2(\mathbb{M}^{(q)},\zeta) = 1 - \sum_{p=1}^{P}\mathbb{M}_p^{(q)}\, e^{i\zeta\kappa_p^q} \simeq 0, \zeta\in\hat{C} \quad \text{or } \sup_{\zeta\in\hat{C}}\left|J_2(\mathbb{M}^{(q)},\zeta)\right| \text{ is minimum.}$$

The interpolation is now independent of both the wavenumber k and the cell size. The $P\times P$ matrix $\mathbb{M}_{p,q} = \mathbb{M}_p^{(q)}$ is the interpolator. It depends only on the $\tilde{\lambda}_p$, $p = 1, ..., P$.

Step 2d: Since the function $\zeta \mapsto e^{i\zeta\kappa_p}$ is analytical on $\hat{C}$, its maximum is reached on the boundary. In practice, we choose to sample the path $\partial\hat{C}$ with N equidistant points ζ_n^N, $n = 1, \dots N$ and we minimize $\displaystyle\sum_{n=1}^{N}\left|J_2(\mathbb{M}^{(q)},\zeta_n^N)\right|^2$.

In summary, for a fixed value of $q = 1, \dots, P$ (i.e. a fixed value of $(\kappa_p^q)_{p=1,\dots,P}$) the best $\mathbb{M}^{(q)}$ in $\mathbb{R}^P$ is found by solving P least square problems of size $P\times 2N$ (the factor 2 coming from the inclusion of both the real and imaginary parts). To illustrate the efficiency of this interpolation we have solved this least square problem with $N = 500$ for each of the 41 laws given by Yarvin and Rokhlin. The maximum of the interpolation error on 10 000 points is always ten times smaller than the quadrature error associated to the law.

5 A wideband `PWFMM`

It is now possible to derive a wideband `PWFMM`. It combines the standard `HF-PWFMM` [9] and the `LF-PWFMM` based on the plane wave expansions (19) and (38); together with the translation functions (25) and (37). The treatment of the fast multipole ("FM") contributions exploits expansion (2) in a manner suggested by their multiplicative form, i.e. in 3 steps. Accordingly in step (i) *multipole moments* defined by

$$\mathcal{F}^{B_s}(\vec{k}) = \sum_{x_s\in B_s} e^{-\mathrm{i}\vec{k}.(x_s-c_{B_s})}\rho(x_s) \tag{40}$$

are computed for each cell B_s. Then, *local expansions* for the cells B_t are evaluated by applying the translation functions T to the multipole moments according to

$$\mathcal{N}^{B_t}(\vec{k}) = \sum_{\substack{B_s=\vec{t}+B_t \\ \vec{t}\in\mathcal{T}}} T(\vec{k};\vec{t})\mathcal{F}^{B_s}(\vec{k}) \tag{41}$$

where $\mathcal{T}$ denotes the set translation vectors (step (ii)). Replacing the integration over $\hat{\Lambda}$ in (2) by a numerical quadrature rule, the "FM" contributions to the potential are now expressed as

$$V^{B_t}(x_t) = \oint_{\hat{\Lambda}} \mathcal{N}^{B_t}(\vec{k}) e^{\mathrm{i}\vec{k}.(x_t - c_{B_t})}, \quad x_t \in B_t. \tag{42}$$

This is the single-level FMM. The computation of V^{B_t} by the multi-level FMM consists of the following five steps:

1. *Initialization*: compute multipole moments for all lowest-level cells.
2. *Upward pass*: recursively aggregate multipole moments by moving upward (via an interpolation and a shift of the cell center) in the tree until level 2 is reached.
3. *Translation*: initialize local expansions for each level-ℓ cell and at each level $2 \leq \ell \leq \pounds$ by translating the multipole moments.
4. *Downward pass*: for all levels $3 \leq \ell \leq \pounds$, the local expansion for each level-ℓ cell is updated (via a shift of the cell center and an inverse interpolation) with the contribution from the parent level-$(\ell-1)$ cell.
5. When the leaf level $\ell = \pounds$ is reached, all local expansions have been computed. The contribution V^{B_t} is evaluated with the level-$\pounds$ quadrature rule.

In the `HF-PWFMM`, $\hat{\Lambda}$ is the unit sphere S^2 of $\mathbb{R}^3$ (up to the factor k) and the filtered translation function is T_L given by

$$T_L(\vec{k};\vec{t}) = \frac{ik}{4\pi} \sum_{m=0}^{L} (2m+1) i^m h_m^{(1)}(k|\vec{t}|) P_m(\cos(\hat{k},\vec{t})) \quad \text{with } \vec{k} = \hat{k}k.$$

Now plugging the translation function defined in (25), i.e. the one associated to the propagative part, in (41) we obtain an approximation of

$$V_p^{B_t}(x_t) = \sum_{x_s} G_p(|x_t - x_s|)\rho(x_s)$$

which corresponds to the contribution of the propagative part of the `LF-PWFMM`. In other words, the only change of translation function in (41) amounts to computing the propagative part $V_p^{B_t}(x_t)$ in the `LF-PWFMM` instead of the "FM" contributions with the `HF-PWFMM`. This similarity between the two algorithms is true only because we have replaced the upper hemisphere by the complete sphere; hence, the same quadrature rule for the `HF-PWFMM` and the `LF-PWFMM` is used. In the case of the multi-level algorithm, the same remark remains valid. The only difference is that the multipole moments and local expansions are computed using the values of the same fields (via an interpolation) but at other levels in the tree. This relationship between the expansions of the Helmholtz Green's function in the `HF-PWFMM` and of the propagative part in the `LF-PWFMM`, is the basis of the combined `HF/LF-PWFMM` we propose.

The algorithm for the evanescent part is very similar. The main difference is that the 316 translation directions are dispatched into six groups (one for each axis of evanescence). Consequently the `PWFMM` algorithm is now applied six times for the evanescent part, the total number of translations being unchanged. Due to the additional cost introduced by the evanescent part, the `LF-PWFMM` is stable at all frequencies but more expensive than the standard `HF-PWFMM`. It is thus natural to use the `HF-PWFMM` whenever possible, i.e. as long as sufficient accuracy is achieved.

In practice, it is possible to associate a boolean for each triplet $(\vec{t}, kd, \varepsilon)$ to define whether the `HF-PWFMM` can be safely applied (according to a prescribed accuracy ε). As a consequence, both the `HF` and `LF` approximations are used at any given level, depending on the values of the translation vector considered. Finally, the algorithm is decomposed into three groups: low frequency formula for all translation vectors (for the small cells at the higher levels), high frequency formula for all the translation vectors (for the large cells at the lower levels) and a combination of the two formulations for the intermediate levels. We will give more details on the practical aspects in a forthcoming paper.

Advantages and drawbacks. In this work a wideband FMM based entirely on the `PWFMM` is proposed. Similarly to what is proposed in [5] or [17] different translation methods are used for the lower and the higher frequencies; but the implementation is significantly simplified since it avoids:

- the conversion between the exponential and partial-wave expansions for the lower frequencies [5];
- the use of spherical harmonic transforms to perform the transition between the low and high frequency formulations [5, 17];

On the other hand, the price to pay is the decomposition of the Helmholtz Green's function for the lower frequencies between a propagative and an evanescent part. This decomposition is actually not a drawback since it simplifies the transition between the low and high frequency formulations. In addition, we have demonstrated theoretically and numerically that it is possible to build two accurate quadrature rules for these two parts while keeping the number of quadrature points reasonable. Of course, the quadrature rule for the evanescent part is not optimal, compared to the Generalized Gaussian quadrature rule proposed in [5]. But by using a clever change of variable in the evanescent part, we are able to use the optimal Generalized Gaussian quadrature rule derived for the static case. To summarize, we list the main advantages:

- all the translation (i.e. multipole-to-local) operators are diagonal;
- the conversion between the low and high frequency formulations boils down to the removal of the evanescent part and the change of translation function;
- no precomputations are needed since only the Generalized Gaussian quadrature rule for the static case is used and no conversions are used.

Finally, it is worth noting that the computational costs for the different approaches are similar: $O(N \log N)$ for the higher frequencies [23] and $O(N)$ for the lower frequencies since the number of quadrature points is bounded in this latter case.

6 Illustration of the accuracy

We consider 3 cylinders (L_1 is the length of the largest one) meshed with triangular surface elements (see Fig. 2). Starting from the initial mesh C_1, the meshed cylinders C_2 (resp. C_3) are obtained via a translation and a scaling with a factor 0.1 (resp. 0.01). Since the edge lengths in this mesh vary from 1 to 100, the `HF-PWFMM` used on this example would lead to inaccurate results. It is necessary to use a wideband FMM.

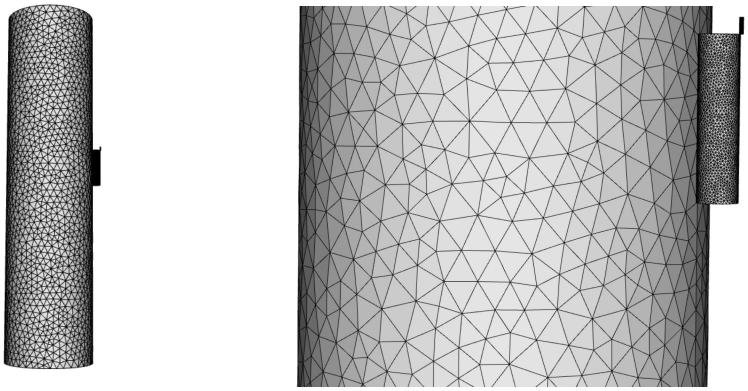

Figure 2: Geometry considered to illustrate the capabilities of the wideband `PWFMM`.

We aim at computing the potential $V(x_t)$ (with x_t the center of gravity of the triangle t) given by

$$V(x_t) = \int_\Gamma G(x_t, y)\rho(y)d\Gamma(y), \quad \text{with } \rho(y) = \frac{\partial}{\partial n(y)} e^{ik\hat{k}\cdot y} \text{ and } \quad \hat{k} = \frac{1}{\sqrt{2}}(\hat{x} + \hat{z}).$$

The wavenumber k is automatically adapted to achieve 10 points per wavelength for the largest edge of the mesh. We discretize, then decompose the integral into near and far contributions

$$V(x_t) = \tilde{\mathbb{G}}_{t,t}\rho_t + \sum_{t \neq T} \mathbb{G}_{t,T}\rho_T, \text{with } \rho_T = ik|T|n_T \cdot \hat{k}\, e^{ik\hat{k}\cdot x_T} \text{ and } \tilde{\mathbb{G}}_{T,T} = \frac{1}{|T|}\int_T G(x_t, y)dT(y).$$

The self term $\tilde{\mathbb{G}}_{t,t}\rho_t$ is computed directly while the second term is computed using the `PWFMM`. Similarly to what is done in [5], in Table 3 we compare the CPU times to evaluate the potential, with the direct method or with the wideband `PWFMM`; we consider two meshes and three prescribed accuracies. We report the relative 2-norm errors between the direct computations and the `PWFMM` on the complete mesh and also on the 3 different cylinders. The octree used by the combined `LF/HF-PWFMM` contains $\pounds = 15$ levels for the two meshes. The `HF-PWFMM` (resp. `LF-PWFMM`) is applied for all the interactions between cells, from the level 3 up to the level $\ell_o - 1$ (resp. from $\ell_o + 1$ to $\pounds$). At level ℓ_o, the `HF-PWFMM` is used except for the directions $(\pm 2, 0, 0), (0, \pm 2, 0), (0, 0, \pm 2)$. The corresponding level ℓ_o is reported in the last column of Table 3. The method is shown to achieve the prescribed levels of accuracy with a drastic reduction of CPU time compared to the direct calculation. In addition, the ratios between the direct and `PWFMM` times are similar to the ones reported in [5].

N_t	L_1	Time direct	Time FMM	2−norm	2−norm on C_1	2−norm on C_2	2−norm on C_3	level ℓ_o LF/HF
420 678	17λ	2h02	28s	$3.3\ 10^{-3}$	$6.7\ 10^{-4}$	$5.2\ 10^{-4}$	$1.0\ 10^{-2}$	12
			43s	$2.7\ 10^{-4}$	$3.1\ 10^{-5}$	$2.5\ 10^{-5}$	$8.5\ 10^{-4}$	10
			87s	$1.3\ 10^{-5}$	$1.3\ 10^{-6}$	$7.4\ 10^{-7}$	$4.2\ 10^{-5}$	7
1 008 102	23λ	11h48	50s	$1.8\ 10^{-3}$	$8.9\ 10^{-4}$	$1.3\ 10^{-3}$	$3.5\ 10^{-3}$	12
			78s	$1.8\ 10^{-4}$	$5.7\ 10^{-5}$	$1.6\ 10^{-4}$	$3.2\ 10^{-4}$	11
			220s	$5.3\ 10^{-6}$	$1.0\ 10^{-6}$	$1.1\ 10^{-6}$	$1.2\ 10^{-5}$	7

Table 3: Comparison of the CPU times to evaluate the potential, with the direct method or with the wideband PWFMM.

7 Conclusions

In this work, we propose some theoretical improvements for the LF-PWFMM to reduce the CPU costs, control the accuracy and justify the method. Following Greengard et al. [16] we decompose the Helmholtz Green's function into a propagative and an evanescent parts. For the propagative part, we establish estimates on the error introduced by the quadrature rule over the unit sphere; we also provide a detailed analysis for the translation function. For the evanescent part, we propose a new plane wave expansion for which error estimates are provided; the novelty of this formulation is to use the quadrature rule of the static case to perform the radial integration. It is thus possible to derive a simple interpolation algorithm based on the FFT, similar to the one for the unit sphere in the HF-PWFMM. We end the paper with the proposition of a wideband PWFMM combining the advantages of the low and high frequency formulations. This wideband FMM is simple to implement (while remaining computationally competitive) because it is based only on plane wave expansions. Its accuracy is illustrated on a numerical example.

The nature of this article is mainly theoretical. The authors are aware that the efficiency of the algorithm has to be confirmed by further numerical results. A forthcoming article, focusing more specifically on numerical aspects, is under way.

Acknowledgment

The work of F. Collino was partially supported under the grant of DGA (REI 2010340001). We thank the authors of [30] for providing, via the internet, the quadrature rule.

References

[1] M. Abramowitz and I. Stegun. *Handbook of Mathematical Functions.* Dover, New-York, 1964.

[2] I. Bogaert and F. Olyslager. A low frequency stable plane wave addition theorem. *J. Comput. Phys.*, 228(4):1000–1016, 2009.

[3] Q. Carayol and F. Collino. Error estimates in the fast multipole method for scattering problems. I. Truncation of the Jacobi-Anger series. *M2AN Math. Model. Numer. Anal.*, 38(2):371–394, 2004.

[4] C. Cecka and E. Darve. Fourier-based fast multipole method for the Helmholtz equation. *SIAM J. Sci. Comput.*, 35(1):A79–A103, 2013.

[5] H. Cheng, W.Y. Crutchfield, Z. Gimbutas, L.F. Greengard, J.F. Ethridge, J. Huang, V. Rokhlin, N. Yarvin, and J. Zhao. A wideband fast multipole method for the Helmholtz equation in three dimensions. *J. Comput. Phys.*, 216(1):300–325, 2006.

[6] W.C. Chew, J.M. Jin, E. Michielssen, and J.M. Song. *Fast and efficient algorithms in computational electromagnetics*. Artech House, 2001.

[7] R. Coifman, V. Rokhlin, and S. Wandzura. The Fast Multipole Method for the Wave Equation: A Pedestrian Prescription. *IEEE Antennas and Propagation Magazine*, 35(3):7–12, 1993.

[8] D. Colton and R. Kress. *Inverse Acoustic and Electromagnetic Scattering Theory*, volume 93. Springer-Verlag, 1992.

[9] E. Darve. The fast multipole method. I. Error analysis and asymptotic complexity. *SIAM J. Numer. Anal.*, 38(1):98–128, 2000.

[10] E. Darve. The fast multipole method: Numerical implementation. *J. Comput. Phys.*, 160(1):196–240, 2000.

[11] E. Darve and P. Havé. Efficient fast multipole method for low-frequency scattering. *J. Comput. Phys.*, 197(1):341–363, 2004.

[12] E. Darve and P. Havé. A fast multipole method for Maxwell equations stable at all frequencies. *Philosophical Transactions of the Royal Society of London. Series A: Mathematical, Physical and Engineering Sciences*, 362(1816):603–628, 2004.

[13] B. Engquist and L. Ying. Fast directional multilevel algorithms for oscillatory kernels. *SIAM J. Sci. Comput.*, 29(4):1710–1737, 2007.

[14] M.A. Epton and B. Dembart. Multipole translation theory for the three-dimensional Laplace and Helmholtz equations. *SIAM J. Sci. Comput.*, 16(4):865–897, 1995.

[15] W. Fong and E. Darve. The black-box fast multipole method. *J. Comp. Phys.*, 228(23):8712–8725, 2009.

[16] L. Greengard, J. Huang, V. Rokhlin, and S. Wandzura. Accelerating fast multipole methods for the Helmholtz equation at low frequencies. *IEEE Comput. Sci. Eng.*, 5(3):32–38, 1998.

[17] N.A. Gumerov and R. Duraiswami. Wideband fast multipole accelerated boundary element methods for the three-dimensional Helmholtz equation. *The Journal of the Acoustical Society of America*, 125(4):2566–2566, 2009.

[18] W. Hackbusch. A sparse matrix arithmetic based on $\mathcal{H}$-matrices. Part I: Introduction to $\mathcal{H}$-matrices. *Computing*, 62(2):89–108, 1999.

[19] M. L. Hastriter, S. Ohnuki, and W.C. Chew. Error control of the translation operator in 3D MLFMA. *Microwave and Optical Technology Letters*, 37(3):184–188, 2003.

[20] P. Havé. *Méthodes multipôles rapides pour l'electromagnétisme : Parallélisme et basses fréquences*. PhD thesis, Université Paris VI, 2004.

[21] B. Lizé. *Résolution Directe Rapide pour les Eléments Finis de Frontière en Electromagnétisme et Acoustique : $\mathcal{H}$-Matrices. Parallélisme et Applications Industrielles*. PhD thesis, Université Paris 13, 2014.

[22] M. Messner, M. Schanz, and E. Darve. Fast directional multilevel summation for oscillatory kernels based on Chebyshev interpolation. *J. Comp. Phys.*, 231(4):1175–1196, 2012.

[23] B. Michiels, J. Fostier, I. Bogaert, and D. De Zutter. Weak scalability analysis of the distributed-memory parallel MLFMA. *IEEE Transactions on Antennas and Propagation*, 61(11):5567–5574, 2013.

[24] S. Ohnuki and W. C. Chew. Numerical accuracy of multipole expansion for 2-D MLFMA. *IEEE Trans. Antennas Propagat.*, 51(8):1883–1890, 2003.

[25] V. Rokhlin. Rapid solution of integral equations of classical potential theory. *J. Comput. Phys.*, 60(2):187–207, 1985.

[26] V. Rokhlin. Diagonal forms of translation operators for the Helmholtz equation in three dimensions. *Applied and Computational Harmonic Analysis*, 1:82–93, 1993.

[27] A. Sommerfeld. Propagation of waves in wireless telegraphy. *Ann. der Physick und Chemie*, 28(3):665–736, 1909.

[28] H. Wallen, S. Jarvenpaa, P. Yla-Oijala, and J. Sarvas. Broadband Müller-MLFMA for Electromagnetic Scattering by Dielectric Objects. *IEEE Transactions on Antennas and Propagation*, 55:1423–1430, May 2007.

[29] G.N. Watson. *A treatise on the theory of Bessel functions*. Cambridge University Press, 1966.

[30] N. Yarvin and V. Rokhlin. Generalized Gaussian quadratures and singular value of integral operators. *SIAM J. Sci. Comput.*, 20(2):699–718, 1998.

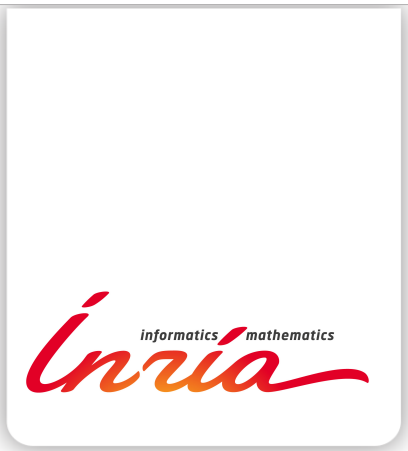

RESEARCH CENTRE
SACLAY – ÎLE-DE-FRANCE

1 rue Honoré d'Estienne d'Orves
Bâtiment Alan Turing
Campus de l'École Polytechnique
91120 Palaiseau

Publisher
Inria
Domaine de Voluceau - Rocquencourt
BP 105 - 78153 Le Chesnay Cedex
inria.fr

ISSN 0249-6399